# Damping of Cosmic Magnetic Fields

Karsten Jedamzik
*Max-Planck-Institut fuer Astrophysik*
*85748 Garching bei Muenchen, Germany*

Višnja Katalinić and Angela V. Olinto
*Department of Astronomy and Astrophysics and Enrico Fermi Institute*
*University of Chicago, 5640 S. Ellis Ave, Chicago, IL 60637*

We examine the evolution of magnetic fields in an expanding fluid composed of matter and radiation with particular interest in the evolution of cosmic magnetic fields. We derive the propagation velocities and damping rates for relativistic and non-relativistic fast and slow magnetosonic, and Alfvén waves in the presence of viscous and heat conducting processes. The analysis covers all MHD modes in the radiation diffusion and the free-streaming regimes. When our results are applied to the evolution of magnetic fields in the early universe, we find that cosmic magnetic fields are damped from prior to the epoch of neutrino decoupling up to recombination. Similar to the case of sound waves propagating in a demagnetized plasma, fast magnetosonic waves are damped by radiation diffusion on all scales smaller than the radiation diffusion length. The characteristic damping scales are the horizon scale at neutrino decoupling ($M_\nu \approx 10^{-4} M_\odot$ in baryons) and the Silk mass at recombination ($M_\gamma \approx 10^{13} M_\odot$ in baryons). In contrast, the oscillations of slow magnetosonic and Alfvén waves get overdamped in the radiation diffusion regime, resulting in frozen-in magnetic field perturbations. Further damping of these perturbations is possible only if before recombination the wave enters a regime in which radiation free-streams on the scale of the perturbation. The maximum damping scale of slow magnetosonic and Alfvén modes is always smaller than or equal to the damping scale of fast magnetosonic waves, and depends on the magnetic field strength and its direction relative to the wave vector.

Our findings have multifold implications for cosmology. The dissipation of magnetic field energy into heat during the epoch of neutrino decoupling ensures that most magnetic field configurations generated in the very early universe satisfy big bang nucleosynthesis constraints. Further dissipation before recombination constrains models in which primordial magnetic fields give rise to galactic magnetic fields or density perturbations. Finally, the survival of Alfvén and slow magnetosonic modes on scales well below the Silk mass may be of significance for the formation of structure on small scales.

## I. INTRODUCTION

In an attempt to explain the origin of galactic magnetic fields through the amplification of primordial fields, several authors have considered scenarios for generating magnetic fields in the early universe [1]. In such scenarios, one attempts to generate fields which will be sufficiently large after recombination at least to seed galactic dynamos and at best to produce galactic fields without dynamo amplification. It is generally assumed that after a primordial field is generated in the early universe, it becomes frozen into the cosmic plasma and redshifts by flux conservation with the expansion of the universe ($B \propto a^{-2}$; $a(t)$ is the cosmic scale factor). This assumption is usually justified by noting that the cosmological plasma is highly conductive and magnetic diffusion is insignificant.

In this paper, we show that this simple picture of magnetic field evolution is incorrect: at certain epochs in the early universe, particularly during recombination and neutrino decoupling, magnetic field energy is converted into heat through the damping of magneto-hydrodynamic (MHD) modes. The damping is caused by dissipation in the fluid, which arises from the finite mean free path of photons or neutrinos.

The physical process by which the MHD modes are damped is analogous to that involved in the damping of density fluctuations around recombination [2], and around neutrino decoupling [3]. Studies of the damping of density fluctuations with no magnetic fields present show that, in the diffusive regime (when the scales of interest are much larger than the mean free path of photons or neutrinos, $l_{\rm mfp}$), the effective viscosity and heat conductivity arising from the finite mean free path cause the damping of acoustically oscillating density perturbations. Since with the expansion of the universe the mean free path of the decoupling particles grows faster than the wavelength of an oscillatory mode, all modes whose wavelengths are smaller than the mean free path around decoupling have previously been in the diffusion regime. The rate of damping in this regime ensures that a wave is significantly damped before the mean free path of the decoupling particles becomes comparable to the wavelength of the mode. For this reason, the investigation of damping in the diffusion regime yields a reasonable estimate of the final damping scales of density fluctuations.

However, when magnetic fields are added to the fluid, the existence of different MHD modes—Alfvén, fast magnetosonic, and slow magnetosonic waves—adds complexity to the problem. We show that while fast magnetosonic waves (which include sound waves) damp efficiently in the diffusion regime by the described process, slow magnetosonic and Alfvén waves may survive damping by diffusion. Slow magnetosonic and Alfvén modes oscillate with frequencies which depend on the strength of the background magnetic field and on its direction relative to the mode's wave vector, and are in general different from the frequency of sound waves of the same wavelength. In the case of a weak background magnetic field or a large angle between the background field and the wave vector, the frequency can be slow enough for the damping by viscosity to overcome the oscillation, producing behavior which resembles an overdamped oscillator and causes the actual damping of the amplitude to be inefficient. The overdamped slow magnetosonic and Alfvén modes therefore survive diffusion damping. However, they undergo additional damping if, with the expansion of the universe, they enter the so called free-streaming regime, i.e. if the mean-free-path grows to be much larger that the wavelength of a mode. As a consequence, whereas fast magnetosonic modes are damped mostly when radiation is diffusing, slow magnetosonic and Alfvén modes can also be significantly damped when radiation is free-streaming. Therefore, when studying the damping of all MHD modes in order to estimate their damping scales, it is necessary to investigate both the free-streaming and the diffusion regimes even before the final stages of the decoupling process.

The damping of MHD modes which causes the dissipation of magnetic energy can be illustrated with the following picture: as long as there exist spatially tangled magnetic fields, Lorentz forces accelerate the fluid, setting up oscillations about a force-free field configuration; the induced motions are damped by the effective viscosity of photons or neutrinos; this causes the exponential decrease in the amplitude of the oscillations and thus results in the straightening of magnetic field lines towards a force-free configuration. After the cosmological magnetic fields undergo this damping process they have little structure on scales below a characteristic damping scale, and the magnetic energy density in such primordial fields is much smaller than that expected from the simple redshift argument above.

In this paper we follow the evolution of MHD modes and derive their propagation velocities and damping rates both in the diffusion and free-streaming regimes during the decoupling of photons and neutrinos. The existence of highly relativistic particles with mean free path much shorter than the wavelength of a MHD mode (e.g., photons and leptons) requires the use of relativistic MHD. In the radiation diffusion regime, studied in §2, we develop a relativistic description of viscous expanding fluids with magnetic fields, while in the free-streaming case, §3, the effects of the photons or neutrinos are included through heat exchange and a drag force which they exert on the fluid. This procedure allows us to calculate, in §4, the maximum damping lengths after the epochs of neutrino decoupling and recombination. Our results may be applied to other astrophysical environments where MHD waves propagate in a viscous fluid, since in the derivation of the dispersion relations we leave the sources of viscosity and heat conductivity unspecified.

## II. DAMPING OF MAGNETOHYDRODYNAMIC MODES IN THE RADIATION DIFFUSION REGIME

When the mean free paths of all interacting particle species are shorter than the wavelength of the MHD mode we are interested in, ($\lambda \gg l_{\rm mfp}$), it is adequate to study the evolution of a single fluid and account for the effect of the diffusing particles by introducing shear viscosity, bulk viscosity, and heat conductivity into the fluid equations [4]. In order to calculate the damping of MHD modes following this approach, we derive linearized relativistic MHD equations of an expanding dissipative fluid. We start by reviewing the equations for a non-ideal relativistic fluid in §2.1, and add the electromagnetic contributions to the fluid equations in §2.2. In §2.3 we calculate the propagation velocities and damping rates for all MHD modes. Our results are applicable for general viscous relativistic and non-relativistic plasmas, as long as the pressure is dominated by radiation pressure.

Throughout the paper we assume that the magnetic field can be decomposed into a large magnitude background component $\mathbf{B}_0(\mathbf{x},t)$, and a small perturbation, $\mathbf{b}(\mathbf{x},t)$. We additionally assume that the curl of the background component is negligible when compared to the curl of the perturbations. These two assumptions allow us to solve for the damping of MHD modes analytically.

The use of scalar viscosities and heat conductivity implicitly neglects any anisotropies in these quantities due to the presence of the magnetic field. Further, since our equations are derived for an isotropically, homogeneously, and adiabatically expanding plasma, the background magnetic field, $\mathbf{B}_0$, is required to have vanishing spatial average on sufficiently large scales, $\langle \mathbf{B}_0 \rangle = 0$. In our derivation we also neglect gravitational forces because the scales of interest are smaller than the Jeans mass scale, and we assume the plasma to be infinitely conducting which is an excellent approximation for most astrophysical plasmas and for the early universe (see, e.g., Ref. [5]).

### A. Relativistic Imperfect Fluids

We consider the evolution of a non-ideal, relativistic fluid in a homogeneously and isotropically expanding background using the spatially flat Robertson-Walker metric $g_{\mu\nu} = \mathrm{diag}(1, -a^2, -a^2, -a^2)$ and comoving coordinates $x^\mu$. The time dependent scale factor $a(t)$ provides the connection between proper (physical) coordinates $x'^\mu$ and the comoving coordinates: $x'^0 = x^0$ and $x'^i = ax^i$ (Greek indices run from 0 to 3 whereas Latin indices run from 1 to 3).

The relativistic fluid is described by the energy-momentum tensor

$$T^{\mu\nu} = T_I^{\mu\nu} + \tau^{\mu\nu} + T_{\mathrm{EM}}^{\mu\nu}, \tag{1}$$

which is separated into three parts: the ideal fluid tensor $T_I^{\mu\nu}$, the non-ideal fluid part $\tau^{\mu\nu}$, which accounts for dissipation, and the electromagnetic energy-momentum tensor $T_{\mathrm{EM}}^{\mu\nu}$ (added in §2.2). The equations of fluid dynamics can be derived from energy-momentum conservation

$$T^{\mu\nu}{}_{;\nu} = 0. \tag{2}$$

In comoving coordinates Eq. 2 becomes

$$\frac{\partial T^{0\mu}}{\partial x^\mu} + \dot{a}a\left(\sum_{i=1,3} T^{ii}\right) + 3\left(\frac{\dot{a}}{a}\right)T^{00} = 0, \tag{3}$$

and

$$\frac{\partial T^{i\mu}}{\partial x^\mu} + 5\left(\frac{\dot{a}}{a}\right)T^{i0} = 0, \tag{4}$$

with the dot representing a derivative with respect to time $x^0$.

The energy-momentum tensor for an ideal fluid is

$$T_I^{\mu\nu} = (\rho + p)U^\mu U^\nu - pg^{\mu\nu}, \tag{5}$$

where $\rho$, $p$, and $U^\mu$ are the total energy density, the total pressure, and the four velocity of the fluid, respectively. The non-ideal contributions to the fluid energy-momentum tensor can be written as [6]

$$\begin{aligned}\tau^{\mu\nu} = {}& \eta\Big(U^{\mu;\nu} + U^{\nu;\mu} - U^\mu U^\lambda U^\nu{}_{;\lambda} - U^\nu U^\lambda U^\mu{}_{;\lambda}\Big) \\ & + \Big(\xi - \frac{2}{3}\eta\Big)U^\lambda{}_{;\lambda}\big(g^{\mu\nu} - U^\mu U^\nu\big) \\ & + \kappa\left[U^\mu\left(\frac{\partial T}{\partial x_\nu} - TU^\nu{}_{;\lambda}U^\lambda\right) + U^\nu\left(\frac{\partial T}{\partial x_\mu} - TU^\mu{}_{;\lambda}U^\lambda\right) - 2U^\mu U^\nu\frac{\partial T}{\partial x_\lambda}U_\lambda\right].\end{aligned} \tag{6}$$

In this expression, $T$ stands for temperature and $\eta$, $\xi$, and $\kappa$ are shear viscosity, bulk viscosity, and heat conductivity respectively.

The effective viscosities and heat conductivity for either photons or neutrinos are given by [7,3,4]:

$$\eta = \frac{4}{15}g\frac{\pi^2}{30}T^4 l_{\mathrm{mfp}}\,, \tag{7}$$

$$\xi = 4g\frac{\pi^2}{30}T^4\left[\frac{1}{3} - \left(\frac{\partial p}{\partial \rho}\right)_n\right]l_{\mathrm{mfp}}\,, \tag{8}$$

$$\kappa = \frac{4}{3}g\frac{\pi^2}{30}T^3 l_{\mathrm{mfp}}\,, \tag{9}$$

where $n$ is the number density of the conserved particles in the fluid and $g$ is the statistical weight of the diffusing particles.

The exact form of $\tau^{\mu\nu}$ is partially a matter of definition since, in relativistic fluid mechanics, the fluid velocity can be defined either by the flow of conserved particles [6] or by the flow of energy [8]. These definitions coincide in non-relativistic fluid mechanics where the rest mass of particles dominates the total energy. In our case, a relativistic one-fluid approximation, the charged and strongly interacting particles (protons, neutrons, electrons, etc.) which compose the fluid are all perfectly coupled and have the same velocity as the conserved particle number, the baryon number. The energy flow may differ from the particle flow, however, due to the energy transported by the imperfectly coupled neutrinos and photons. We choose to follow the velocity of the charged particles (and, therefore, the flow of baryon number) which appears explicitly in the magneto-hydrodynamic equations below.

The conservation of particle number can be written as

$$n^{\mu}{}_{;\mu} = 0, \tag{10}$$

where $n^{\mu} = nU^{\mu}$ is the particle number four-current with the proper number density of particles $n$. The particle number we follow is the net baryon number, $n^{b}$, which is conserved for temperatures below the electroweak transition.

We can now derive the linearized equations of ordinary relativistic fluid dynamics in an expanding universe from Eq. 2 - 10, by expanding the fluid variables around their background values

$$\rho(\mathbf{x},t) = \rho_0(t) + \rho_1(\mathbf{x},t), \tag{11}$$
$$p(\mathbf{x},t) = p_0(t) + p_1(\mathbf{x},t), \tag{12}$$
$$T(\mathbf{x},t) = T_0(t) + T_1(\mathbf{x},t), \tag{13}$$
$$n^b(\mathbf{x},t) = n_0^b(t) + n_1^b(\mathbf{x},t), \tag{14}$$
$$U^{\mu} = U_0^{\mu} + U_1^{\mu} \ . \tag{15}$$

The four-velocity is that of a stationary fluid element (with respect to the comoving frame) plus a small velocity perturbation

$$U_0^{\mu} = \big(1,0,0,0\big), \quad U_1^{\mu} = \big(0,\frac{\mathbf{v}}{a}\big). \tag{16}$$

We choose $U_1^{\mu}$ in this particular form so that the fluid velocity in proper coordinates, $\mathbf{v}' = (\dot{a}/a)\mathbf{x}' + \mathbf{v}$, corresponds to an isotropic expansion plus an additional peculiar velocity $\mathbf{v}$. We consider fluids in which the peculiar velocities are much smaller than the speed of light, e.g. $|\mathbf{v}| \ll 1$ with velocities are measured in units of the speed of light. Although the fluid velocities are small, a relativistic treatment is necessary to adequately account for the presence of relativistic particles (e.g., photons and neutrinos).

Evaluating equations 2 and 10 to lowest order in the fluid variables, we obtain

$$\frac{\partial\rho_0}{\partial t} + 3\left(\frac{\dot{a}}{a}\right)(\rho_0 + p_0) = 9\xi\left(\frac{\dot{a}}{a}\right)^2, \tag{17}$$

which represents conservation of entropy when $\xi = 0$, and

$$\frac{\partial n_0^b}{\partial t} + 3\left(\frac{\dot{a}}{a}\right)`n_0^b = 0, \tag{18}$$

which represents conservation of baryon number. If we expand the energy momentum tensor and baryon number four-current to first order in the perturbation variables $U_1^{\mu}$, $\rho_1$, $p_1$, $T_1$, and $n_1^b$, use Eq. 3–4, and subtract the zeroth order solution, we obtain

$$\frac{\partial\rho_1}{\partial t} + (\rho_0 + p_0)\frac{1}{a}\nabla\cdot\mathbf{v} + 3\left(\frac{\dot{a}}{a}\right)(\rho_1 + p_1 - 2\xi\nabla\cdot\mathbf{v}) - \frac{\kappa}{a^2}\nabla^2 T_1 - \frac{\kappa}{a^2}\frac{\partial}{\partial t}(aT_0\nabla\cdot\mathbf{v}) = 0, \tag{19}$$

$$\frac{1}{a^4}\frac{\partial}{\partial t}\left[a^4(\rho_0 + p_0)\mathbf{v} - \kappa a^3\left[\frac{\partial}{\partial t}(aT_0\mathbf{v}) + \nabla T_1\right] - 3\xi a^3\dot{a}\mathbf{v}\right] + \frac{1}{a}\nabla p_1 - \frac{\eta}{a^2}\nabla^2\mathbf{v} - \frac{1}{a^2}(\xi + \frac{1}{3}\eta)\nabla(\nabla\cdot\mathbf{v}) = 0, \tag{20}$$

and

$$\frac{\partial n_1^b}{\partial t} + \frac{n_0^b}{a}\nabla\cdot\mathbf{v} + 3\left(\frac{\dot{a}}{a}\right)n_1^b = 0. \tag{21}$$

These equations form a complete set describing the evolution of a non-ideal fluid; Eq. 19 represents the first law of thermodynamics in local form, Eq. 20 is the relativistic version of Euler's equation, and Eq. 21 represents the conservation of baryon number.

### B. Magneto-Hydrodynamics with Dissipation

We now include the electromagnetic fields. In an inertial frame (denoted by $\hat{}$) the Maxwell tensor has the form

$$\hat{F}^{\mu\nu} = \begin{pmatrix} 0 & E_x & E_y & E_z \\ -E_x & 0 & B_z & -B_y \\ -E_y & -B_z & 0 & B_x \\ -E_z & B_y & -B_x & 0 \end{pmatrix}, \tag{22}$$

where $E_i$ and $B_i$ are the electric and magnetic fields as seen by an observer in the inertial frame. The Maxwell tensor in comoving coordinates ($x^\mu$) can be derived from the Maxwell tensor in inertial coordinates ($\hat{x}^\mu$),

$$F^{\mu\nu} = \Lambda^\mu{}_\lambda \Lambda^\nu{}_\sigma \hat{F}^{\lambda\sigma} \ , \tag{23}$$

where

$$\Lambda^\mu{}_\nu = \frac{\partial x^\mu}{\partial \hat{x}^\nu} \ . \tag{24}$$

The coordinate transformation which transforms the locally Minkowski metric $\hat{g}^{\mu\nu} = \mathrm{diag}(1, -1, -1, -1)$ into the Robertson-Walker metric $g^{\mu\nu} = \mathrm{diag}(1, -1/a^2, -1/a^2, -1/a^2)$ has

$$\Lambda^\mu{}_\nu = \mathrm{diag}(1\,,\,1/a\,,\,1/a\,,\,1/a\,) \ . \tag{25}$$

Thus, in the comoving basis $F^{\mu\nu}$ is

$$F^{\mu\nu} = \begin{pmatrix} 0 & E_x/a & E_y/a & E_z/a \\ -E_x/a & 0 & B_z/a^2 & -B_y/a^2 \\ -E_y/a & -B_z/a^2 & 0 & B_x/a^2 \\ -E_z/a & B_y/a^2 & -B_x/a^2 & 0 \end{pmatrix}. \tag{26}$$

The equations of motion for the electromagnetic fields are Maxwell's equations

$$F^{\mu\nu}{}_{;\nu} = 4\pi J^\mu \tag{27}$$

and

$$\frac{\partial}{\partial x^\lambda} F_{\mu\nu} + \frac{\partial}{\partial x^\nu} F_{\lambda\mu} + \frac{\partial}{\partial x^\mu} F_{\nu\lambda} = 0 \ , \tag{28}$$

where $J^\mu$ is the electric four-current.

In the limit of infinite electrical conductivity, the electric field in the rest frame of the charged particles vanishes:

$$E^\mu = F^{\mu\nu} U_\nu = 0. \tag{29}$$

This condition evaluated in the comoving frame using Eqs. 16 and 26 becomes

$$\mathbf{E} = -\mathbf{v} \times \mathbf{B}. \tag{30}$$

We decompose the magnetic field into its background value, $\mathbf{B}_0$, and a small-amplitude perturbation, $\mathbf{b}(\mathbf{x}, t)$

$$\mathbf{B}(\mathbf{x}, t) = \mathbf{B}_0(\mathbf{x}, t) + \mathbf{b}(\mathbf{x}, t), \tag{31}$$

and impose the following conditions

$$\mathbf{b}(\mathbf{x}, t) \ll \mathbf{B}_0(\mathbf{x}, t) \ , \tag{32}$$

$$\nabla \times \mathbf{B}_0(\mathbf{x}, t) \ll \nabla \times \mathbf{b}(\mathbf{x}, t) \ . \tag{33}$$

We can now derive the relevant Maxwell's equations to zeroth and first order in the small quantities $\mathbf{v}$ and $\mathbf{b}$ by using Eqs. 26, 28, and 30. This yields:

$$\nabla \cdot \mathbf{b} = 0, \tag{34}$$

$$\frac{1}{a^2}\frac{\partial}{\partial t}(a^2\mathbf{b}) = \frac{1}{a}\nabla \times (\mathbf{v} \times \mathbf{B}_0), \tag{35}$$

$$\frac{\partial}{\partial t}(a^2\mathbf{B}_0) = 0. \tag{36}$$

Eq. 36 shows that the background field $\mathbf{B}_0$, by flux conservation, redshifts as $1/a^2$ with the expansion of the fluid.

To complete the system of equations needed to describe the evolution of the fluid in the presence of electromagnetic fields, we must add the contribution from the electromagnetic energy-momentum tensor $T^{\mu\nu}_{\rm EM}$ to the conservation of energy-momentum (Eqs. 3 and 4). The energy-momentum tensor for electromagnetism is

$$T^{\mu\nu}_{\rm EM} = \frac{1}{4\pi}\Big\{F^{\mu\sigma}F^{\nu}{}_{\sigma} - \frac{1}{4}g^{\mu\nu}F^{\sigma\rho}F_{\sigma\rho}\Big\}, \tag{37}$$

which in comoving coordinates becomes

$$T^{\mu\nu}_{\rm EM} = \frac{1}{4\pi}\begin{pmatrix} A & \mathbf{S} \\ \mathbf{S} & \sigma^{ij}\end{pmatrix}, \tag{38}$$

with

$$A = \frac{\big(\mathbf{E}^2 + \mathbf{B}^2\big)}{2}, \quad \mathbf{S} = \frac{\big(\mathbf{E}\times\mathbf{B}\big)}{a}, \quad \text{and} \quad \sigma^{ij} = \frac{1}{a^2}\Big(-E_iE_j - B_iB_j + \frac{1}{2}\delta_{ij}\big(\mathbf{E}^2 + \mathbf{B}^2\big)\Big). \tag{39}$$

We can now evaluate the contributions from the electromagnetic stresses to the conservation of entropy Eq. 17, the first law of thermodynamics in local form Eq. 19, and the relativistic version of Euler's equation Eq. 20. The contribution to the left-hand-side of the zeroth order Eq. 17 is

$$\frac{1}{8\pi a^4}\frac{\partial}{\partial t}(a^4\mathbf{B}_0^2), \tag{40}$$

while to first order in $\mathbf{v}$ and $\mathbf{b}$, the electromagnetic stresses to be added to the left-hand-sides of Eqs. 19 and 20 are

$$\frac{1}{4\pi}\left[\frac{1}{a^4}\frac{\partial}{\partial t}(a^4\mathbf{b}\cdot\mathbf{B}_0) + \frac{\mathbf{B}_0^2}{a}(\nabla\cdot\mathbf{v}) - \frac{1}{a}\big(\mathbf{B}_0\cdot\nabla\big)\big(\mathbf{v}\cdot\mathbf{B}_0\big)\right]. \tag{41}$$

for Eq. 19, and

$$\frac{1}{4\pi a^4}\frac{\partial}{\partial t}\Big(a^4\mathbf{B}_0\times\big(\mathbf{v}\times\mathbf{B}_0\big)\Big) + \frac{1}{4\pi a}\Big[\mathbf{B}_0\times\big(\nabla\times\mathbf{b}\big)\Big], \tag{42}$$

for Eq. 20. After substituting Maxwell's equations (Eq. 34–36) into Eq. 41, we find that the electromagnetic contribution to Eq. 19 is zero. Similarly, Eq. 40 is identical to zero by virtue of Eq. 36 so that both Eq. 17 and 19 are unmodified. The only coupling between the field and the fluid to first order occurs through the velocity of charged particles and the curl of the magnetic field.

Note that the first term of Eq. 42 is only important in the relativistic limit. For a mode with frequency $\omega$ and wavenumber $k$, Eq. 35 implies $\omega b \sim k\bar{v}B$. Therefore, the relative contribution of the first term in Eq. 42 compared to the second term is of order $(\omega/k)^2$. Hence, the first term can only be neglected when the group velocity of a mode, $\partial\omega/\partial k \approx \omega/k$, is much smaller than the speed of light.

To first order in the quantities $T_1$, $n_1^b$, $\rho_1$, $p_1$, $\mathbf{v}$, $\mathbf{b}$, Eqs. 19, 21, 34–36, together with the equation obtained by adding Eq. 42 to the left-hand-side of Eq. 20 describe magneto-hydrodynamics in an expanding fluid. The following definitions help to rewrite our equations into a more convenient form

$$\delta \equiv \frac{T_1}{T_0}, \quad \Delta \equiv \frac{n_1^b}{n_0^b}, \tag{43}$$

$$\tilde{\mathbf{b}} \equiv \frac{\mathbf{b}}{\big(4\pi(\rho_r + p_r)\big)^{\frac{1}{2}}}, \quad \tilde{\mathbf{B}}_0 \equiv \frac{\mathbf{B}_0}{\big(4\pi(\rho_r + p_r)\big)^{\frac{1}{2}}}, \tag{44}$$

$$\eta' \equiv \frac{\eta}{3(\rho_r + p_r)} \ , \quad \xi' \equiv \frac{\xi}{3(\rho_r + p_r)} \ , \quad \kappa' \equiv \frac{\kappa T}{3(\rho_r + p_r)} \ , \tag{45}$$

where $\rho_r = g\pi^2 T_0^4/30$ and $p_r = \rho_r/3$ are the average energy density and pressure of relativistic particles, and $g$ is the total statistical weight of relativistic particles.

For a fluid comprised of baryons and relativistic particles (e.g., photons, neutrinos, $e^{\pm}$-pairs, etc.), the energy density and pressure up to first order in the small quantities are given by

$$\begin{aligned} \rho &= \rho_0 + \rho_1 \\ &= \rho_r\big(1 + 4\delta\big) + \rho^b\big(1 + \Delta\big) \ , \end{aligned} \tag{46}$$

$$\begin{aligned} p &= p_0 + p_1 \\ &= p_r\big(1 + 4\delta\big) \ , \end{aligned} \tag{47}$$

where $\rho_b = n_0^b m_{\mathrm{N}}$ is the baryon energy density, and $m_{\mathrm{N}}$ is the nucleon rest mass. In writing Eq. 47, we assume that baryonic pressure is negligible in comparison to radiation pressure. In this case, and when $\xi = 0$, Eq. 17 and Eq. 18 imply simple redshift relations for the temperature $T_0 \sim 1/a$ and the baryon number density $n_0^b \sim 1/a^3$. We also define

$$R(t) \equiv \frac{3\rho_b}{4\rho_r} \tag{48}$$

as a measure of the relative importance of baryon mass density with respect to energy density in relativistic particles. For $R \to 0$, both energy density and pressure are dominated by relativistic particles, whereas for $R \gg 1$ the energy density is dominated by the baryon rest mass and the pressure is dominated by radiation.

In terms of the newly defined variables, the equations of magneto-hydrodynamics become

$$\dot{\delta} + 36\xi'\left(\frac{\dot{a}}{a}\right)^2\delta + \frac{1}{3a}\nabla\cdot\mathbf{v} - 6\left(\frac{\dot{a}}{a}\right)\frac{\xi'}{a}\nabla\cdot\mathbf{v} - \frac{\kappa'}{a^2}\nabla^2\delta - \frac{\kappa'}{a}\frac{\partial}{\partial t}\nabla\cdot\mathbf{v} = 0 \ , \tag{49}$$

$$\begin{aligned} \left(\frac{\partial}{\partial t} + 36\xi'\left(\frac{\dot{a}}{a}\right)^2\right)\left((1+R)\mathbf{v} - 3\kappa'\big(\dot{\mathbf{v}} + \frac{1}{a}\nabla\delta\big) - 9\xi'\big(\frac{\dot{a}}{a}\big)\mathbf{v}\right) + \frac{1}{a}\nabla\delta - \frac{3\eta'}{a^2}\left(\nabla^2\mathbf{v} + \frac{1}{3}\nabla(\nabla\cdot\mathbf{v})\right) \\ - \frac{3\xi'}{a^2}\nabla(\nabla\cdot\mathbf{v}) + \tilde{\mathbf{B}}_0 \times \left(\frac{\partial\mathbf{v}}{\partial t} \times \tilde{\mathbf{B}}_0\right) + \frac{1}{a}\tilde{\mathbf{B}}_0 \times \big(\nabla \times \tilde{\mathbf{b}}\big) = 0 \ , \end{aligned} \tag{50}$$

$$\frac{\partial}{\partial t}\tilde{\mathbf{b}} = \frac{1}{a}\nabla\times\big(\mathbf{v} \times \tilde{\mathbf{B}}_0\big) \ , \tag{51}$$

$$\nabla\cdot\tilde{\mathbf{b}} = 0 \ , \tag{52}$$

$$\frac{\partial}{\partial t}\tilde{\mathbf{B}}_0 = 0 \ . \tag{53}$$

### C. Dispersion Relations

In order to calculate propagation velocities and damping rates, we first derive the dispersion relations for the different MHD modes by Fourier transforming all perturbative variables ($\delta$, $\Delta$, $\mathbf{b}$, and $\mathbf{v}$, generically represented by $\phi$ below) using the convention

$$\phi(\mathbf{x},t) = \int d^3\mathbf{k}\,\phi(\mathbf{k},t)\exp\big(i\mathbf{k}\cdot\mathbf{x}\big) \tag{54}$$

in which $\mathbf{k}$ is a constant comoving wave vector.

The time dependence of $\phi(\mathbf{k},t)$ is modified by the expansion of the fluid which introduces a time variation into the frequency and the amplitude of the modes. With this in mind it is convenient to write

$$\phi(\mathbf{k},t) = \phi_{\mathbf{k}}(t) \exp\Big[\int i\omega(t)\, dt\Big]. \tag{55}$$

The decrease of the amplitude due to damping is included in the exponential part through imaginary solutions for $\omega$ while the explicit time dependence of $\phi_{\mathbf{k}}(t)$ acounts only for the effects of the expansion.

The system of equations resulting from the substitution of Eq. 54 into Eqs. 49–53 is solved separately for the different MHD modes: Alfvén waves, for which the density and the temperature of the fluid are uniform and the velocity of the fluid is perpendicular to the background magnetic field ($\mathbf{k} = k\hat{\mathbf{x}}, \mathbf{B}_0 = B_x\hat{\mathbf{x}} + B_z\hat{\mathbf{z}}, \mathbf{b} = b\hat{\mathbf{y}}, \mathbf{v} = v\hat{\mathbf{y}}$ and $\delta = 0$); and magnetosonic waves, for which the velocity of the fluid makes an arbitrary angle with the background field ($\mathbf{k} = k\hat{\mathbf{x}}, \mathbf{B}_0 = B_x\hat{\mathbf{x}} + B_y\hat{\mathbf{y}}, \mathbf{b} = b\hat{\mathbf{y}}, \mathbf{v} = v_x\hat{\mathbf{x}} + v_y\hat{\mathbf{y}}$). Note that sound waves, which propagate along the background field without affecting it ($\mathbf{B}_0 \parallel \mathbf{k} \parallel \mathbf{v}$ and $\mathbf{b} = 0$), are a special case of magnetosonic waves. In all dispersion relations and their solutions, $\theta$ denotes the angle between the background magnetic field and the wave vector.

The dispersion relation for magnetosonic modes allows two solutions: slow magnetosonic modes and fast magnetosonic modes. Fast magnetosonic modes are similar in nature to sound waves, while slow magnetosonic modes are closer to Alfvén waves. This fact plays an important role in the damping of magnetosonic waves, and is apparent for weak magnetic fields ($\rho_B \ll \rho_{\text{fluid}}$) where fast magnetosonic modes oscillate with $\mathbf{v}$ almost along the direction of $\mathbf{k}$ and involve oscillating density perturbations, while slow magnetosonic modes oscillate almost perpendicularly to $\mathbf{k}$ and have close to vanishing density perturbations. In the special case $\mathbf{k} \parallel \mathbf{B}_0$ fast magnetosonic waves become sound waves and there are no slow magnetosonic solutions. (For a discussion of MHD modes see, for example, Ref. [9].)

We obtain the dispersion relations by substituting Eq. 55 into Eqs. 49–52. The dispersion relations are derived to first order in $\kappa'$, $\eta'$, $\xi'$, which corresponds to the lowest non-trivial expansion in powers of $l_{\text{mfp}}/\lambda$ (where $\lambda$ is the wavelength of a mode). We use the WKB approximation neglecting the time derivatives of the Fourier amplitudes, $\partial\phi_{\mathbf{k}}(t)/\partial t \ll \omega$, and the time derivative of the frequency, $\partial\omega/\partial t \ll -\omega^2$, which arises from the $\partial^2\mathbf{v}/\partial t^2$ term in Eq. 50. This approximation is valid for modes with oscillation frequencies much higher than the expansion rate, $\omega \gg H$.

This procedure for Alfvén waves yields:

$$3\omega^3\kappa' + i\omega^2\left(1 + R + \tilde{B}_0^2\right) + \omega\left(\frac{\dot{a}}{a}R + 3\eta'\left(\frac{k}{a}\right)^2\right) - i\tilde{B}_0^2 cos^2\theta\left(\frac{k}{a}\right)^2 = 0\ . \tag{56}$$

Complete dispersion relations for all MHD modes are, due to their length, placed in Appendix A.

In the following two sections, we present the solutions for oscillation frequencies and damping rates derived from the dispersion relations in the following two limits: the oscillatory limit, when the solution is oscillatory with an exponentially decaying amplitude; and the overdamped limit, when the amplitude of modes exponentially decrease without completing an oscillation.

### *1. Oscillatory Limit*

The solutions to the dispersion relations, $\omega$, generally consist of a real and an imaginary part, which represent the oscillation frequency and the damping rate, respectively. In the oscillatory limit, the dissipative effects are such that the fluid oscillates many times as it damps, $\mathrm{Re}\,\omega \ll \mathrm{Im}\,\omega$. In this case, the dispersion relations can be solved by considering all the viscosity and heat conductivity terms as perturbations on the ideal fluid dispersion relation.

The solutions to the dispersion relations will be conveniently expressed in terms of the speed of sound:

$$v_s = \sqrt{\left(\frac{\partial p}{\partial \rho}\right)_S} = \frac{1}{\sqrt{3(1+R)}}\ , \tag{57}$$

and the relativistic Alfvén speed:

$$v_A = \frac{\tilde{B}_0}{\sqrt{1 + R + \tilde{B}_0^2}}\ . \tag{58}$$

The relativistic Alfvén speed includes the magnetic field energy density in the denominator, which ensures that for strong magnetic fields the Alfvén speed does not exceed the speed of light.

For all modes in the oscillatory limit we first solve the dispersion relations for an ideal fluid and then compute the first order contributions from the dissipative terms. For clarity, all the solutions in their general form have been placed in Appendix A. In this and the following section we give the solutions for each MHD mode in the cosmologically relevant limit of weak magnetic fields ($\tilde{B}_0 \ll 1$) and negligible redshift terms ($\dot{a}/a$).

For weak magnetic fields, the leading terms in the frequencies for fast magnetosonic waves do not depend either on the magnetic field strength or on the direction of propagation, and are therefore the same as the frequencies for sound waves:

$$\omega_{\rm osc}^{\rm FM} = \pm v_s \left(\frac{k}{a}\right) + i\left(\frac{R^2}{2(1+R)^2}\kappa' + \frac{2}{1+R}\eta' + \frac{3}{2(1+R)}\xi'\right)\left(\frac{k}{a}\right)^2 + O(\tilde{B}_0^2). \tag{59}$$

This reproduces the solution for propagation and damping of sound waves given in Ref. [4]. Similarly, the frequencies of slow magnetosonic waves and Alfvén waves are identical to leading order in $B_0$ and have the following form:

$$\omega_{\rm osc}^{\rm SM,A} = \pm v_A \cos\theta \left(\frac{k}{a}\right) + \frac{3}{2} i \frac{\eta'}{(1+R)}\left(\frac{k}{a}\right)^2 + O(\tilde{B}_0^2)\ . \tag{60}$$

The solutions show that, while for small magnetic fields the damping of slow magnetosonic and Alfvén waves proceeds through shear viscosity, fast magnetosonic waves are damped by shear and bulk viscosity, as well as heat conductivity. Furthermore, fast magnetosonic waves damp differently in different regimes: they damp predominantly by heat conductivity when the matter density is larger than the radiation density, and by shear viscosity when the radiation density dominates. Note that after taking the time dependence of all variables into account, the expansion of the fluid affects the frequencies directly through $\dot{a}/a$ terms (see Appendix A), and indirectly through the integral in Eq. 55. For instance, as in the case of sound waves when $R \ll 1$, the oscillation frequency of a fast magnetosonic mode with a given wavelength in a radiation dominated expansion is twice the frequency of the same wavelength mode in a static background metric.

### *2. Overdamped Limit*

When dissipative effects become very strong, oscillations of MHD modes are inhibited and the evolution of a given MHD mode is dominated by the exponential decay of its amplitude with time. We seek solutions in the extremely overdamped regime by expanding the equations in powers of $\mathrm{Re}\,\omega_{\rm osc}/\mathrm{Im}\,\omega_{\rm osc}$, where $\omega_{\rm osc}$ is the frequency of a wave derived in the oscillatory limit.

In general, a dispersion relation expanded in powers of $\mathrm{Re}\,\omega_{\rm osc}/\mathrm{Im}\,\omega_{\rm osc}$ has several solutions distinguished in nature by their initial conditions. For example, in the case of Alfvén waves, fast decaying solutions arise from initial conditions such that when the velocities of the fluid are damped away by shear viscosities the amplitude of the magnetic perturbations vanish as well. In contrast, when initial conditions generate slowly decaying Alfvén modes, the fluctuations are not erased as the velocities damp to zero; after the damping of fluid motions, the remaining magnetic forces tend to accelerate the fluid, although inefficiently because of the strong viscous damping. Since energy dissipation rates are proportional to the peculiar fluid velocity, the timescale for dissipation of the magnetic field perturbation of slow decaying modes may be extremely large.

While the amplitudes of the fast decaying modes damp at rates similar to the ones calculated in the oscillatory regime (§2.3.1), the amplitudes of slowly decaying modes decay at significantly different rates. For weak magnetic fields ($\tilde{B}_0 \ll 1$), the decay rate for the amplitude of overdamped slow magnetosonic modes is

$$\omega_{\rm od}^{\rm SM} = i\kappa' v_A^2 \left(\frac{k}{a}\right)^2 + i\frac{v_A^2\cos^2\theta}{3\eta'}\ , \tag{61}$$

and the decay rate for Alfvén modes is

$$\omega_{\rm od}^{\rm A} = i\frac{v_A^2\cos^2\theta}{3\eta'}\ . \tag{62}$$

Note that all modes with relativistic propagation velocities ($\mathrm{Re}\,\omega_{\rm osc} \sim k/a$) never enter the overdamped regime in the diffusion limit. For this reason a discussion of overdamped relativistic sound and fast magnetosonic waves is not necessary.

## III. DAMPING OF MAGNETOHYDRODYNAMIC MODES IN THE RADIATION FREE-STREAMING LIMIT

Slow magnetosonic and Alfvén modes which become overdamped during the diffusion regime survive the damping and with the expansion of the universe enter the free-streaming regime when the mean free path of the decoupling particles grows to be larger than the wavelength of a mode. In order to investigate the additional damping that these modes undergo in the free-streaming regime, we study the general case of MHD in an expanding fluid in the presence of a uniform background. Similar to our analysis of the diffusion regime, we study the evolution of a single dissipative fluid. However, in this case the fluid is comprised of all the particles with mean free paths much shorter than the wavelength of the MHD mode, while the decoupling particle species, whose mean free path is now large as it decouples from the rest of the fluid, represents a uniform background on the scales of interest. The dissipation arises from occasional collisions of the fluid particles with the relativistic background.

We generically define a drag coefficient $\alpha$ and a heat exchange coefficient $\gamma$ in the following way: the drag force per unit volume on the fluid element from scattering with the background particles is given by

$$\mathbf{f} \equiv -\alpha \mathbf{v} \rho_{\text{fluid}} \ , \tag{63}$$

and the heat exchanged between the fluid element and the background is

$$\frac{\partial \rho_{\text{thermal}}}{\partial t} \equiv -\gamma \frac{T_1}{T_0} \rho_{\text{thermal}} \ . \tag{64}$$

The exact form of these coefficients is obtained by calculating the transfer of momentum and heat per scattering and averaging it over the distribution of background and fluid particles. We presented the coefficients later separately for neutrino decoupling and photon decoupling.

In order to derive the free-streaming fluid equations, we use the fluid equations developed in §2, as well as techniques for finding solutions described therein. The heating rate from Eq. 64 is incorporated into Eq. 19, while the drag force from Eq. 63 is added to Eq. 20 together with the magnetic field contribution from Eq. 42. Although the local thermodynamic equilibrium between the fluid and the free-streaming component does not hold in general, we consider the case in which the mean scattering time between particles of the fluid component and the free-streaming component is shorter than the characteristic expansion time scale of the fluid. In this case the temperature and velocity of the background is the same as the average temperature and velocity of the fluid. All other assumptions, including non-relativistic fluid velocities, are carried over from §2.

The resulting equations are:

$$\frac{\partial \rho_1}{\partial t} + \frac{1}{a}(\rho_0 + p_0)\nabla \cdot \mathbf{v} + 3\frac{\dot{a}}{a}(\rho_1 + p_1) = -\gamma \frac{T_1}{T_0} \rho_{\text{thermal}} \ , \tag{65}$$

$$\frac{1}{a^4}\frac{\partial}{\partial t}(a^4(\rho_0 + p_0)\mathbf{v}) + \frac{1}{a}\nabla p_1 + \frac{1}{4\pi}\tilde{\mathbf{B}}_0 \times \left(\frac{\partial \mathbf{v}}{\partial t} \times \tilde{B}_0\right) + \frac{1}{4\pi}\tilde{\mathbf{B}}_0 \times (\nabla \times \tilde{\mathbf{b}}) = -\alpha \mathbf{v} \rho_0 \ , \tag{66}$$

$$\frac{\partial n_1^b}{\partial t} + 3\frac{\dot{a}}{a} n_1^b + \frac{n_0^b}{a}\nabla \cdot \mathbf{v} = 0 \tag{67}$$

and together with Maxwell's equations Eqs. 51 - 53 they form a complete set.

In order to derive dispersion relations for a given fluid, we have to specify the energy density, matter density, and pressure, and substitute these into the above set of equations. This is done in the rest of §3 for two fluid combinations: a baryonic fluid with free-streaming photons; and a fluid which consists of baryons and relativistic particles like photons and $e^+e^-$ pairs, in a background of free-streaming neutrinos. All the dispersion relations as well as the solutions for fast magnetosonic modes are given in the appendices. Here we present the solutions to dispersion relations for slow magnetosonic modes and Alfvén modes, the two modes that in the presence of weak magnetic fields survive into the free-streaming regime before recombination.

### A. Neutrino Free-Streaming Limit

Around neutrino decoupling the fluid consists of tightly coupled baryons, photons, and $e^+e^-$ pairs. The dominant component of the pressure is radiation pressure,

$$p_r = \frac{1}{3}\rho_r, \tag{68}$$

and, since $R \simeq 0$, the speed of sound is

$$v_s = \frac{1}{\sqrt{3}} \, . \tag{69}$$

The energy density (equal to $\rho_{\rm thermal}$) has contributions from all relativistic particles, counted in the number of degrees of freedom $g_r$,

$$\rho_r = g_r \frac{\pi^2}{30} T^4 . \tag{70}$$

The heat exchange coefficient and the drag coefficient, defined by Eq. 64 and Eq. 63, are approximately the same at the high temperatures of neutrino free-streaming. Computed by averaging the transfer of energy in each scattering over a distribution of background particles and a distribution of fluid particles [10], they are:

$$\gamma \simeq \sigma_w n_w \frac{\rho_\nu}{\rho_\gamma} = \frac{g_\nu}{g_r l_\nu} \tag{71}$$

and

$$\alpha \simeq \gamma \, . \tag{72}$$

Here $\sigma_w$ is the cross section for scattering of neutrinos with other weakly interacting particles, $n_w$ is the number density of weakly interacting particles (scatterers), $g_\nu$ is the neutrino statistical weigth, and $l_\nu$ is the neutrino mean free path.

Following the steps used in the diffusion regime (§2.3), we obtain dispersion relations for the different MHD modes and present them in Appendix B.

### *1. Oscillatory Limit*

The oscillation frequencies and damping rates for slow magnetosonic and Alfvén modes are again obtained by first solving the dispersion relations for an ideal fluid and then solving for the first order dissipative terms. In terms of the previously defined Alfvén speed, the solutions for small magnetic fields are the same for slow magnetosonic and Alfvén modes, and have the form:

$$\omega_{\rm osc}^{\rm SM,A} = \pm v_A \cos\theta \left(\frac{k}{a}\right) + \frac{3i}{8}\alpha \, . \tag{73}$$

The frequencies for oscillatory fast magnetosonic waves (including sound waves) are presented in Appendix B.

### *2. Overdamped Limit*

As in the diffusion regime, the solutions in the extremely overdamped regime ($\mathrm{Re}\,\omega_{\rm osc} \ll \mathrm{Im}\,\omega_{\rm osc}$) are derived by expanding the equations in powers of $\mathrm{Re}\,\omega_{\rm osc}/\mathrm{Im}\,\omega_{\rm osc}$. The overdamped solution in the case of weak magnetic fields is, for slow magnetosonic modes

$$\omega_{\rm od}^{\rm SM} = \frac{i}{4}\gamma v_A^2 + \frac{4 i v_A^2 \cos^2\theta}{3\alpha} \left(\frac{k}{a}\right)^2 , \tag{74}$$

and for Alfvén waves

$$\omega_{\rm od}^{\rm A} = \frac{4 i v_A^2 \cos^2\theta}{3\alpha} \left(\frac{k}{a}\right)^2 . \tag{75}$$

As in the case of radiation diffusion (§2.3), relativistic fast magnetosonic modes do not become overdamped in the free-streaming regime.

### B. Photon Free-Streaming Limit

Fluid equations for the modes in the free-streaming limit around photon decoupling are somewhat different from the cases analyzed so far. Namely, the only contribution to the energy density of the perturbations is the thermal energy density of baryons,

$$\rho_{\rm thermal} = \frac{3}{2}(n_e + n_p)T = 3n_b T, \tag{76}$$

which enters Eq. 65 but can be neglected in Eq. 66 because it is much smaller than the matter density. Here $n_e$ and $n_p$ are electron and proton number densities respectively. Furthermore, since the photons can be considered decoupled on the free-streaming scales, the only pressure left to support the oscillations is the pressure of the baryonic fluid itself:

$$p_b = (n_e + n_p)T = 2n_b T. \tag{77}$$

This yields the gradient of pressure in Eq. 66 which depends both on density and temperature fluctuations and is best expressed through the sound speed:

$$\frac{1}{\rho}\nabla p = \frac{3}{5}c_s^2(\nabla\Delta + \nabla\delta), \tag{78}$$

where $c_s$ is the adiabatic baryonic speed of sound for a fully ionized proton-electron fluid,

$$c_s = \sqrt{\left(\frac{\partial p_b}{\partial \rho_b}\right)_S} = \sqrt{\frac{10}{3}\frac{T}{m_p}}\ . \tag{79}$$

With these substitutions for the densities and the pressure, we obtain dispersion relations for different MHD modes and present them in Appendix C.

The drag and heat exchange coefficients, which appear in the dispersion relations and their solutions, are similarly obtained as in the neutrino free-streaming case, and have the following form [11]:

$$\alpha \simeq \sigma_{\rm T} n_e \frac{\rho_\gamma}{\rho_b} = \frac{1}{l_\gamma R}, \tag{80}$$

and

$$\gamma \simeq \frac{m_p}{m_e}\alpha. \tag{81}$$

#### 1. *Oscillatory Limit*

Unlike in the relativistic cases where the photon pressure dominates, the structure of the non-relativistic equations with free-streaming photons allows for oscillating magnetosonic modes with two different propagation velocities and damping rates. These modes are commonly referred to as adiabatic and isothermal, depending if heat transport is slow or rapid compared to the oscillation time: a mode is adiabatic when $\omega \gg \gamma$ and $\omega \gg \alpha$, and it is isothermal when $\gamma \gg \omega \gg \alpha$. Alfvén modes have only one solution since they do not include density or temperature fluctuations and therefore are not affected by heat transport.

Again we derive the dispersion relations from Eqs. 51–53 and Eqs. 65–67, and place them in Appendix C. Before presenting the solutions for slow magnetosonic and Alfvén modes, it is useful to introduce the non-relativistic Alfvén speed,

$$c_A = \frac{\tilde{B}_0}{\sqrt{R}}\ . \tag{82}$$

The oscillation frequency and the damping rate for slow magnetosonic waves in the adiabatic regime ${\rm Re}\,\omega \gg \gamma, \alpha$ are given by:

$$\omega_{\rm osc}^{\rm SM} = \pm c_A \cos\theta \left(\frac{k}{a}\right) + i\left(\frac{\alpha}{2} + \frac{\gamma}{5}\frac{\tilde{B}_0 \sin^2\theta}{c_s^2 R}\right) , \tag{83}$$

and

$$\omega_{\rm osc}^{\rm SM} = \pm c_s \cos\theta \left(\frac{k}{a}\right) + i\left(\frac{\alpha}{2} + \frac{\gamma}{5}\right) , \tag{84}$$

where the upper solution corresponds to weak magnetic fields such that $c_s \gg c_A$ and the lower solution to strong magnetic fields with $c_s \ll c_A$. It is important to remember that both of these solutions are derived for a background magnetic field whose energy density is much smaller than the energy density in photons. The condition for adiabaticity is dependent on the strength of the magnetic field since oscillation frequencies of magnetosonic waves are different for strong and weak magnetic fields.

Slow magnetosonic modes in the isothermal regime, $\gamma \gg \mathrm{Re}\,\omega \gg \alpha$, have the solution

$$\omega_{\rm osc}^{\rm SM} = \pm c_A \cos\theta \left(\frac{k}{a}\right) + i\frac{\alpha}{2}, \tag{85}$$

and

$$\omega_{\rm osc}^{\rm SM} = \pm\sqrt{\frac{3}{5}} c_s \cos\theta \left(\frac{k}{a}\right) + i\frac{\alpha}{2}, \tag{86}$$

where again the upper solution is for $c_s \gg c_A$ and the lower solution is for $c_s \ll c_A$.

The result for Alfvén waves is

$$\omega_{\rm osc}^{\rm A} = \pm c_A \cos\theta \left(\frac{k}{a}\right) + i\frac{\alpha}{2}. \tag{87}$$

The frequency of non-relativistic fast magnetosonic waves in the adiabatic and isothermal limits are placed in Appendix C.

### *2. Overdamped Limit*

The frequencies for slow magnetosonic waves corresponding to slow exponential decay are:

$$\omega_{\rm od}^{\rm SM} = i\frac{c_A^2 \cos^2\theta}{\alpha}\left(\frac{k}{a}\right)^2 , \tag{88}$$

and

$$\omega_{\rm od}^{\rm SM} = i\frac{3c_s^2 \cos^2\theta}{5\alpha}\left(\frac{k}{a}\right)^2 , \tag{89}$$

with the upper solution for $c_A \ll c_s$, and the lower solution for $c_A \gg c_s$. The slowly decaying mode of overdamped Alfvén waves has frequency

$$\omega_{\rm od}^{\rm A} = i\frac{c_A^2 \cos^2\theta}{\alpha}\left(\frac{k}{a}\right)^2 . \tag{90}$$

In contrast to relativistic MHD, some non-relativistic fast magnetosonic modes can enter the overdamped regime. Their damping rates can also be found in Appendix C.

## IV. DAMPING OF MAGNETIC FIELDS IN THE EARLY UNIVERSE

In this section we discuss the implications of the damping of magneto-hydrodynamic modes for the evolution of cosmological magnetic fields. Magnetic fields generated in the early universe are likely to be randomly oriented, spatially varying fields with small coherence lengths, usually of the order of the horizon at the epoch when the fields were created. We assume that the magnetic fields are created with magnetic field energy below equipartition with the radiation energy density, i.e. $\tilde{B}_0 \ll 1$. For an arbitrary magnetic field configuration, we choose a separation of scales such that in a given volume the field can be described as an approximately force-free background magnetic field $\mathbf{B}_0$, and a spectrum of propagating modes $\mathbf{b}(\mathbf{k})$, where $|\mathbf{b}| \ll |\mathbf{B}_0|$. In this case we can decompose the propagating modes into slow and fast magnetosonic, and Alfvén modes with different wave vectors $\mathbf{k}$ and different phases. Although the condition $|\mathbf{b}| \ll |\mathbf{B}_0|$ may not be easily achieved for every field configuration, the predicted evolution of propagating modes is indicative of the general field evolution. In particular, the efficient viscous damping discussed in this paper should cause the dissipation of magnetic energy in generic field configurations.

We are interested in the evolution of individual MHD modes from before the epoch of neutrino decoupling to recombination. For each epoch we wish to determine the characteristic scales over which pre-existing cosmic magnetic fields are damped. As previously described, the evolution of fast magnetosonic waves is distinctively different from the evolution of slow magnetosonic modes and Alfvén waves; therefore they are discussed separately: fast magnetosonic waves in §4.1, and slow magnetosonic and Alfvén waves in §4.2.

For the calculation of the damping scales we need the expressions for the mean free path of the decoupling particles as well as the ratio of the baryon density to the photon density. While the universe cools from temperatures below the electroweak breaking scale ($T \sim 100$ GeV) to neutrino decoupling ($T_\nu \sim$ MeV), neutrinos are the particles with the longest mean free path and therefore the most efficient momentum and heat transporters. The neutrino mean free path at temperature $T$ can be written as

$$l_\nu(T) \simeq \frac{1}{G_F^2 T^2 (n_l + n_q)} \simeq 10^{11}\mathrm{cm}\left(\frac{T}{\mathrm{MeV}}\right)^{-5}\left(\frac{g_l + g_q}{8.75}\right)^{-1}, \tag{91}$$

where $n_l$ and $n_q$ are lepton and quark number densities, $G_F$ is Fermi's constant, and $G_F^2 T^2$ is a typical weak interaction cross section. The quantities $g_l$ and $g_q$ are the statistical weights of relativistic weakly interacting leptons and quarks present at the epoch of interest.

At temperatures below the completion of the $e^+e^-$-annihilation ($T \sim 20$ keV), heat and momentum are most efficiently transported by photons. The dominant process limiting the photon mean free path during this period is Thomson scattering of photons off electrons which gives the photon mean free path the following form:

$$l_\gamma(T) \simeq \frac{1}{\sigma_T n_e} \simeq 10^{22}\mathrm{cm}\left(\frac{T}{0.25\mathrm{eV}}\right)^{-3}\left(\frac{\Omega_b h^2}{0.0125}\right)^{-1} X_e(T)^{-1}, \tag{92}$$

where $X_e$ is the number of free electrons per baryon, $\sigma_T$ is the Thomson cross section, and $n_e$ is the electron density.

The damping of MHD waves is particularly efficient during the epochs of neutrino decoupling and recombination, when efficient momentum transfer and heat transport arise from the quickly growing mean free path of the decoupling particles. Therefore, all the variables in the above equations have been scaled to their values at those epochs. Also, since at neutrino decoupling the dominant scattering process is scattering of neutrinos off leptons, the appropriate values for the parameters in Eq. 91 are $g_l = 8.75$ ($e^\pm$ and six neutrino species) and $g_q = 0$. The remaining unspecified parameter, the ionization fraction $X_e$, drops within a short time from 1 to $\sim 10^{-5}$ during recombination which occurs approximately at $T_\gamma^d \simeq 0.25$ eV.

The baryon mass density is negligible when compared to the radiation energy density during neutrino decoupling ($R \approx 0$), while around recombination it is approximately given by

$$R = \frac{3\rho_b}{4\rho_r} \approx 0.4\left(\frac{T}{0.25\mathrm{eV}}\right)^{-1}\left(\frac{\Omega_b h^2}{0.0125}\right), \tag{93}$$

where $\Omega_b$ is the fractional contribution of baryons to the closure density and $h$ is the present Hubble constant in units of 100 km s$^{-1}$ Mpc$^{-1}$. In writing Eq. 93 we implicitly assume that neutrinos have decoupled from the remaining particle species.

### A. Damping of Fast Magnetosonic Waves in the Early Universe

The damping of all fast magnetosonic modes is to leading order equivalent to the damping of sound waves if the energy density in the large-scale magnetic field is much smaller than the energy density in radiation. The damping occurs due to the diffusion of either neutrinos prior to neutrino decoupling, or photons before recombination. From the expressions in Eqs. 91 and 92, which represent mean free paths in proper units, it can be seen that in both cases the comoving mean free path grows with the expansion of the universe. As a consequence, MHD modes with wavelengths $\lambda_p = 2\pi a(T)/k$ smaller than the mean free path $l_{\rm mfp}(T)$ at time $t(T)$ were in the diffusion regime at some prior time in the early universe, i.e. $\lambda_p(T') \gg l_{\rm mfp}(T')$ at $t(T')$ .

The amount of damping that fast magnetosonic modes undergo in the diffusion regime can be calculated using the damping rates in Eq. 59. From the leading damping term, $2i\eta'(k/a)^2/(1+R)$, and the definitions in Eqs. 45 and 7, we see that the amplitude of the perturbation is damped between time $t = 0$ and $t$ by

$$\exp\left(-\int_0^t \frac{l_{\rm mfp}}{\lambda_p^2}{\rm d}t'\right). \tag{94}$$

If we define a characteristic damping scale as the largest comoving wavelength of an MHD mode whose initial amplitude has been damped by at least one e-folding by time $t$, this damping scale approximately corresponds to the comoving photon/neutrino diffusion length,

$$d^2 = \int_0^t \frac{l_{\rm mfp}(t')}{a^2(t')}{\rm d}t', \tag{95}$$

which is the distance a photon/neutrino has random walked between time $t = 0$ and $t$.

In this section we present all the damping scales in comoving units, in particular, comoving to the present epoch, unless stated otherwise. The diffusion damping scale calculated for fast magnetosonic waves prior to neutrino decoupling ($T \geq 1$ MeV) is:

$$\lambda_\nu^{\rm FM} \simeq 2\times 10^{20}{\rm cm}\left(\frac{T}{\rm MeV}\right)^{-\frac{5}{2}}\left(\frac{g_r}{10.75}\right)^{-\frac{3}{4}}\left(\frac{g_\nu}{5.25}\right)^{\frac{1}{2}}\left(\frac{g_l+g_q}{8.75}\right)^{-\frac{1}{2}}. \tag{96}$$

Note that the damping scale at neutrino decoupling converted to proper units approximately corresponds to the causal horizon at that time, $\lambda_\nu({\rm MeV}) \approx 5\times 10^{10}{\rm cm}$ .

In a similar fashion we can compute the comoving damping scale of fast magnetosonic waves due to the effects of the finite photon mean free path at lower temperatures. Around recombination, where we assume matter domination, this damping scale is

$$\lambda_\gamma^{\rm FM} \simeq 7\times 10^{25}\,{\rm cm}\left(\frac{T}{0.25{\rm eV}}\right)^{-\frac{5}{4}}\left(\frac{\Omega_b h^2}{0.0125}\right)^{-\frac{1}{2}}(\Omega_0 h^2)^{-\frac{1}{4}}. \tag{97}$$

In this expression $\Omega_0$ is the total density in units of the critical density at the present epoch.

Baryonic mass scales can be associated with the damping length scales by defining

$$M \equiv \frac{4\pi}{3}\rho_b(T)\left(\frac{\lambda(T)a(T)}{2}\right)^3, \tag{98}$$

where $\rho_b$ is the average baryon mass density at temperature $T$. The baryonic mass scale associated with the damping scale of fast magnetosonic waves by neutrino diffusion around neutrino decoupling is

$$M_\nu^{\rm FM} \simeq 10^{-4}{\rm M}_\odot\left(\frac{T_\nu}{\rm MeV}\right)^{-\frac{15}{2}}\left(\frac{g_r}{10.75}\right)^{-\frac{9}{4}}\left(\frac{g_\nu}{5.25}\right)^{\frac{3}{2}}\left(\frac{g_l+g_q}{8.75}\right)^{-\frac{3}{2}}\left(\frac{\Omega_b h^2}{0.0125}\right), \tag{99}$$

and by photon diffusion around recombination

$$M_\gamma^{\rm FM} \simeq 10^{13}{\rm M}_\odot\left(\frac{T_\gamma}{0.25{\rm eV}}\right)^{-\frac{15}{4}}\left(\frac{\Omega_b h^2}{0.0125}\right)^{-\frac{1}{2}}(\Omega_0 h^2)^{-\frac{3}{4}}. \tag{100}$$

The above calculations for the damping scales are approximate in that we assume that the damped modes are in the diffusion regime, $l_{\nu,\gamma} \ll \lambda_p$. The diffusion approximation is not a valid approximation late within the decoupling epochs. Around neutrino decoupling, while our analysis uncovers the order of magnitude of the damping mass scale, an improvement on the diffusion approximation only, would not yield more accurate results since the calculated damping scale approximately corresponds to the causal horizon at that time. Around recombination, our treatment is analogous to the calculations of the damping of sound waves in Ref. [4]; in writing Eq. 97 we assume an instantaneous recombination while the ionization fraction $X_e$ decreases gradually to zero during recombination. More detailed treatments for the damping of sound waves during recombination have been performed using the Boltzman equation [12–14] or using a two-fluid model [15,16]. Since the dominant damping terms of fast magnetosonic waves are the same as those of sound waves, values for the sound wave damping scale calculated in more accurate models may be used as better approximations to the fast magnetosonic damping scale. A review of previous Silk scale calculations is given in Ref. [14].

### B. Damping of Slow Magnetosonic and Alfvén Waves in the Early Universe

Unlike the damping of fast magnetosonic waves, the damping of slow magnetosonic and Alfvén waves in the early universe proceeds through several different stages. We illustrate these stages by following an Alfvén wave from after neutrino decoupling up to recombination.

Initially, in the diffusion regime where $\lambda \gg l_{\rm mfp}$, a wave oscillates and damps in the same manner as described for fast magnetosonic waves. The oscillation frequency and the damping rate are shown in Eq. 60, and after using Eqs. 45 and 7 they approximately become

$$\omega_{\rm osc}^{\rm A} \simeq \pm v_A \left(\frac{k}{a}\right) \cos\theta + i l_\gamma \left(\frac{k}{a}\right)^2 . \tag{101}$$

The damping rate in this expression is the same as the damping rate for fast magnetosonic modes, and is valid as long as $v_A \cos\theta \gg l_\gamma k/a$. The crucial difference, however, is that for a small background magnetic field in the early universe, the oscillation frequency of an Alfvén mode $(v_A k/a)$ is much smaller than the oscillation frequency of a fast magnetosonic mode with the same wavelength $(v_s k/a)$. While all fast magnetosonic modes of interest satisfy the condition for damping in the oscillatory regime $(v_s \gg l_\gamma k/a)$, an Alfvén mode can become overdamped when, with the expansion of the universe, the mean-free-path becomes large enough for dissipative effects to overcome the oscillation $(v_A cos\theta \simeq l_\gamma k/a)$. One may define a temperature dependent wavelength $\lambda_{\rm od}$,

$$\lambda_{\rm od}(T, B_0) \simeq \frac{2\pi l_\gamma(T)}{v_A \cos\theta} , \tag{102}$$

such that modes with proper wavelength $\lambda_p \geq \lambda_{\rm od}$ are oscillatory while modes with $\lambda_p \leq \lambda_{\rm od}$ are overdamped.

Overdamped modes are a superposition of fast and slowly decaying overdamped modes, and the relative amplitudes depend on the phase of the mode when it becomes overdamped. Fast decaying overdamped modes damp at rates similar to the oscillatory modes, and therefore their damping is equivalent to the damping of fast magnetosonic modes discussed in the previous section. In this section, we follow the significantly different evolution of the slowly decaying overdamped modes which experience the least damping. The amplitude of a slowly decaying overdamped Alfvén mode damps with a rate given by Eq. 62, which in terms of the photon mean-free-path is

$$\omega_{\rm od}^{\rm A} \simeq i \frac{v_A^2 \cos^2\theta}{l_\gamma} . \tag{103}$$

Since the damping rate is inversely proportional to the growing mean free path, the integrated damping rate is much smaller than the integrated damping rate of fast magnetosonic modes during the same period. As a result, the damping in overdamped diffusion is inefficient and the damping scales of Alfvén modes at the end of the diffusion regime are smaller than the damping scales of fast magnetosonic modes.

The left-hand-side of Fig. 3 (left of the dotted line) illustrates the evolution of Alfvén waves in the diffusion regime for $\cos\theta = 1$ and a background magnetic field of $\tilde{B}_0 \approx 10^{-3}$ (corresponding to $B_0 \approx 3 \times 10^{-9}$ Gauss at present). In the diffusion regime there are two important temperature dependent scales: the photon diffusion length scale (dashed line), which is the scale damped by one e-folding by the time the universe cools to temperature $T$ provided that modes are still in the oscillatory regime; and the overdamping length scale given by Eq. 102 (solid line), which shows the temperature at which a mode with comoving wavelength $\lambda_c$ enters the overdamped regime. The modes which do not damp significantly in the radiation diffusion regime before they become overdamped, preserve their amplitude until they reach the free-streaming regime, apart from small additional damping during the transition itself. On the graph, these are all the modes with comoving wavelength larger than that given by the intersection of the solid line with the dashed line. Therefore, the intersection of these two lines roughly represents the largest Alfvén mode that is damped by one e-folding in the diffusion regime. Its position depends on the strength of the background magnetic field and on the angle between the field and the wave vector.

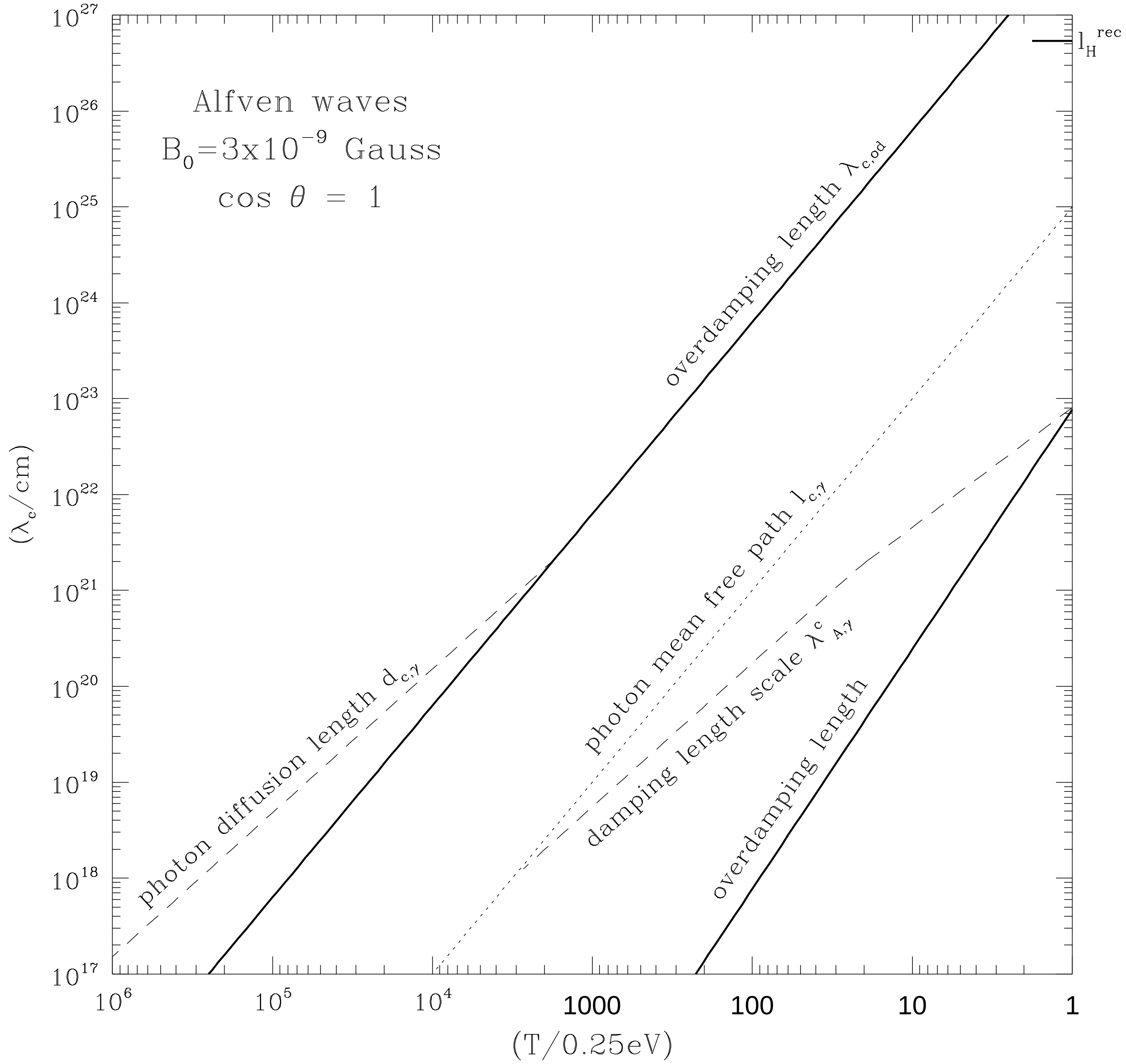


FIG. 1. Scales relevant for the evolution of Alfvén and slow magnetosonic waves before recombination, calculated for modes that propagate at $\cos\theta = 1$ and a background magnetic field of $B_0 = 3 \times 10^{-9}$Gauss today. All length scales are given in comoving units. Any mode with fixed comoving wavelength $\lambda_c$ will at cosmic temperature $T$ be in the photon diffusion regime if it is to the left of the dotted line, or in the photon free-streaming regime if it is to the right. Modes with wavelength $\lambda_c$ will at temperature $T$ be non-oscillatory (overdamped) if they are between the two solid lines. The two dashed lines indicate the temperature at which a mode of given wavelength is damped by one e-fold, either during its oscillatory evolution in photon diffusion or its overdamped evolution in photon free-streaming. The figure assumes $\Omega_b = 0.0125$ and $h = 1$, and equality between radiation and matter energy density at $T_{\rm EQ} = 5.5$eV. See §4.2 for a more detailed explanation.

Some overdamped modes enter the free-streaming regime before recombination (to the right of the dotted line in Fig. 3) as the mean free path of the decoupling particles grows with the expansion. The dissipation coefficients in the free-streaming regime are inversely proportional to the mean free path unlike those in the diffusion regime. This implies that, when a wave enters the free-streaming regime, it is initially overdamped and becomes oscillatory when the drag force and the heat conduction decrease as the mean free path increases. It also implies that modes in the free-streaming regime undergo most damping while overdamped. The damping rates during free-streaming, derived using Eq. 80 in Eqs. 87 and 90, are:

$$\omega_{\rm od}^{\rm A} \simeq i c_A^2 l_\gamma \left(\frac{\rho_b}{\rho_\gamma}\right)\left(\frac{k}{a}\right)^2 \cos^2\theta \ , \tag{104}$$

when a wave is overdamped, and

$$\omega_{\rm osc}^{\rm A} \simeq \pm c_A \left(\frac{k}{a}\right) \cos\theta + i\frac{1}{l_\gamma}\frac{\rho_\gamma}{\rho_b}. \tag{105}$$

when it oscillates.

Using Eq. 104 in Eq. 55, we find that for Alfvén waves during overdamped free-streaming, the largest comoving wavelength whose amplitude is damped by one e-folding at time $t$ is:

$$(\lambda_\gamma^{\rm A}(t))^2 = \int_0^t c_A^2 \cos^2\theta \, R(t')\frac{l_\gamma(t')}{a^2(t')}{\rm d}t' = c_A^2 \cos^2\theta \, d_\gamma^2(t) R(t) \ , \tag{106}$$

where $d_\gamma(t)$ is the comoving photon diffusion length. As we can see, the damping depends on the strength of the background magnetic field and the angle between the field and the wave vector. The above damping length evaluated at recombination is the characteristic Alfvén wave damping length for the free-streaming regime, because all modes stay overdamped before recombination regardless of the strength of the magnetic field.

The damping of Alfvén waves with free-streaming photons is illustrated on the right-hand side of Fig. 3. The dashed line shows the damping scale from Eq. 106. The solid line marks the transition from overdamped to oscillatory behavior, defined in the same fashion as in the diffusion regime (Eq. 102), with the overdamped region to the left of the line. Since all the modes that cross the dashed line before recombination get damped by one e-folding during overdamped free-streaming, the length scale marked by this line at recombination represents the free-streaming damping scale for Alfvén modes.

In our analysis we have assumed the WKB approximation. This approximation does not formally hold during all the discussed epochs for every mode. In particular, the approximation breaks down for comoving wavelengths between the damping length scale for Alfvén waves in the photon free-streaming regime, $\lambda_\gamma^{\rm A}$, and the photon mean free path (i.e., between the dashed and dotted lines on the right-hand-side of Fig. 4). Although the damping rates calculated in the preceding section predict no damping in this region, some damping is in principle possible since here WKB is not a good approximation. In Fig. 4 we present the result of a numerical integration of the magnetic field amplitude of Alfvén waves in different wavelengths through the epoch of interest. The mode with the largest wavelength which still damps before the epoch of recombination ($T \simeq 0.25$eV) is consistent with our analytic estimate. Note that in this calculation we assume that recombination never occurs (i.e., $X_e \simeq 1$ for $T \leq 0.25$eV in Fig. 4). We have extended the calculation into this non-physical regime to learn when the results obtained by the WKB approximation deviate significantly from the numerical results. From the plot we see that significant discrepancies happen only with modes that would damp after recombination if $X_e$ was kept fixed.

The damping of slow magnetosonic waves proceeds similarly to the illustrated damping of Alfvén waves except for two differences. First, slow magnetosonic waves in overdamped diffusion damp at a slightly different rate than Alfvén waves because of the additional damping expressed through the extra term in Eq. 61. This damping is relevant only for the waves that propagate at very large angles with respect to the background magnetic field. Second, the damping rates for slow magnetosonic waves during free-streaming depend on whether the non-relativistic sound speed is larger or smaller than the non-relativistic Alfvén velocity (Eq. 88–Eq. 89). The damping scale when $c_s > c_A$ is the same as the damping scale for Alfvén waves, while the damping scale for $c_s < c_A$ is unique to slow magnetosonic modes.

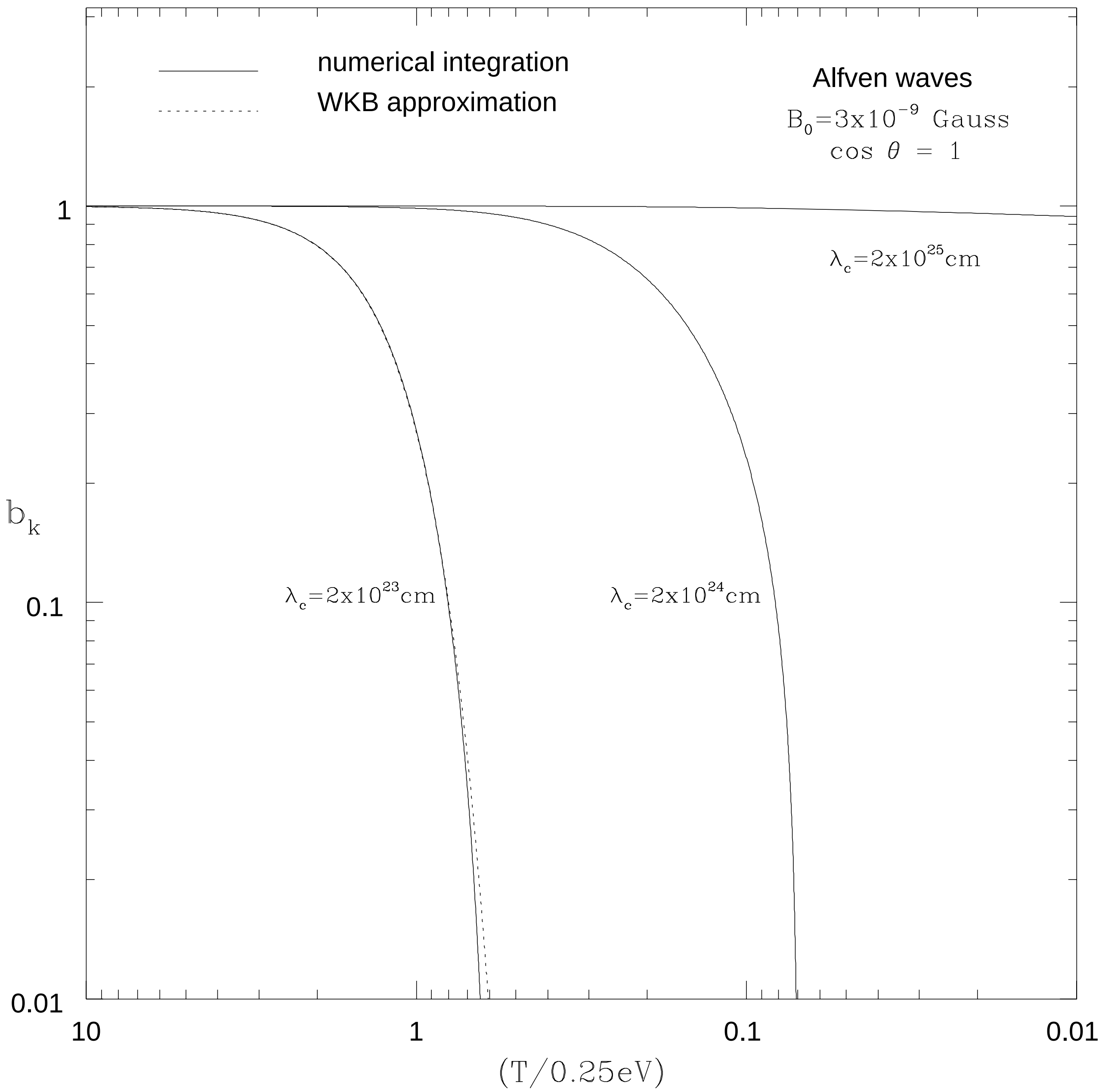


FIG. 2. The evolution of the Fourier amplitude as a function of cosmic temperature calculated numerically (solid line), and analytically using the WKB approximation (dashed line), for Alfven waves with three different comoving wavelengths indicated on the figure. For the calculation we assume $B_0 = 3 \times 10^{-9}$Gauss, $\cos\theta = 1$, $\Omega_b = 0.0125$, and $h = 1$, and we have fixed the ionization fraction at $X_e = 1$ even for temperatures below the approximate temperature of recombination $T \approx 0.25eV$. The largest scale which the numerical calculation shows to be damped by one e-fold before recombination (at ), corresponds to the analytically calculated length scale of $2 \times 10^{23}$ cm.

We can define damping length and mass scales for Alfvén and slow magnetosonic waves analogously to the previous section, and consider that the waves below these scales would have dissipated by the time of neutrino/photon decoupling. The general evolution of all the damping length scales with temperature, followed through the different damping stages up to decoupling, can be found in Appendix D. In this section we present the final damping lengths at neutrino decoupling ($T \simeq 1$MeV) and at recombination ($T \simeq 0.25$eV), for the background magnetic field below $3 \times 10^{-9}$ Gauss, which is the current estimate of the upper limit on magnetic fields on Mpc scales (see, e.g. Ref. [17]).

The final damping scale of Alfvén waves for this range of the background magnetic field strengths is determined by the free-streaming damping length. At neutrino decoupling, most modes in free-streaming are damped while overdamped, although the largest modes are damped just as they begin to oscillate again. This determines the comoving damping scale at neutrino decoupling to be:

$$\lambda_\nu^{\rm A} \simeq 10^{17}{\rm cm}\, B_9 \cos\theta \left(\frac{g_r}{10.75}\right)^{-1} \left(\frac{g_\nu}{5.25}\right)^{\frac{1}{3}} \left(\frac{g_l+g_q}{8.75}\right)^{\frac{1}{3}} . \tag{107}$$

The background magnetic field is expressed through $B_9 = B_0/(3\times10^{-9}{\rm Gauss})$, where $B_0$ is the background magnetic field strength scaled to the present epoch. During photon decoupling, the largest Alfvén mode damped by one e-folding during free-streaming is damped while still in the overdamped regime, and its comoving wavelength is:

$$\lambda_\gamma^{\rm A} \simeq 2\times10^{23}{\rm cm}\, B_9 \cos\theta \left(\Omega_0 h^2\right)^{-\frac{1}{4}} \left(\frac{\Omega_b h^2}{0.0125}\right)^{-\frac{1}{2}} . \tag{108}$$

The baryonic mass scales which correspond to the damping length scales at neutrino and photon decoupling are

$$M_\nu^{\rm A} \simeq 10^{-13}{\rm M}_\odot\, B_9^3 \cos^3\theta \left(\frac{\Omega_b h^2}{0.0125}\right) \left(\frac{g_r}{10.75}\right)^{-3} \left(\frac{g_\nu}{5.25}\right) \left(\frac{g_l+g_q}{8.75}\right) \tag{109}$$

and

$$M_\gamma^{\rm A} \simeq 10^{6}{\rm M}_\odot\, B_9^3 \cos^3\theta \left(\Omega_0 h^2\right)^{-\frac{3}{4}} \left(\frac{\Omega_b h^2}{0.0125}\right)^{-\frac{1}{2}} . \tag{110}$$

The characteristic damping length scale for slow magnetosonic waves at neutrino decoupling is the same as the damping length of Alfvén waves (Eq. 107). At recombination however, the slow magnetosonic damping scale depends on the value of the non-relativistic sound speed relative to the non-relativistic Alfvén speed. When $c_s > c_A$ the damping scale for slow magnetosonic waves in the free-streaming regime is the same as the damping scale for Alfvén waves (Eq. 108). On the other hand, when $c_s < c_A$ the slow magnetosonic damping scale is:

$$\lambda_\gamma^{\rm SM} \simeq 3\times10^{21}{\rm cm}\, \cos\theta \left(\Omega_0 h^2\right)^{-\frac{1}{4}} , \tag{111}$$

which is independent of the background magnetic field strength. The condition $c_s > c_A$ is equivalent to $B_0 \lesssim 5\times10^{-11}\,(\Omega_b h^2/0.0125)^{1/2}$Gauss for the strength of the large scale magnetic field at the present epoch, or $\tilde{B}_0 \lesssim 2\times10^{-5}\,(\Omega_b h^2/0.0125)^{1/2}$ and $B_9 \lesssim 1.7\times10^{-2}\,(\Omega_b h^2/0.0125)^{1/2}$ for the two different scalings of the magnetic field strength present in our equations.

The baryonic mass scales associated with the damping lengths of slow magnetosonic modes are:

$$M_\nu^{\rm S} \simeq 10^{-13}{\rm M}_\odot\, B_9^3 \cos^3\theta \left(\frac{\Omega_b h^2}{0.0125}\right) \left(\frac{g_r}{10.75}\right)^{-3} \left(\frac{g_\nu}{5.25}\right) \left(\frac{g_l+g_q}{8.75}\right) , \tag{112}$$

and

$$M_\gamma^{\rm SM} \simeq \begin{cases} 10^{6}{\rm M}_\odot\, B_9^3 \cos^3\theta \left(\Omega_0 h^2\right)^{-\frac{3}{4}} \left(\frac{\Omega_b h^2}{0.0125}\right)^{-\frac{1}{2}} & \text{for } c_s > c_A \\ 1{\rm M}_\odot\, \cos^3\theta \left(\Omega_0 h^2\right)^{-\frac{3}{4}} \left(\frac{\Omega_b h^2}{0.0125}\right) & \text{for } c_s < c_A \end{cases} \tag{113}$$

## V. CONCLUSIONS

In this paper we have studied the effects of dissipation on the propagation of MHD modes in an expanding fluid composed of matter and radiation. We have derived the propagation velocities and damping rates for fast and slow magnetosonic, and Alfvén waves in the radiation diffusion and radiation free-streaming regimes. The derived damping rates have general applications in magnetized relativistic and nonrelativistic astrophysical environments. We have applied the damping rates to the evolution of MHD modes in the early universe to show that cosmic magnetic fields suffer significant damping from before neutrino decoupling to the end of recombination.

Fast magnetosonic waves are damped by radiation diffusion on all scales smaller than the radiation diffusion length in analogy to the propagation of sound waves in a demagnetized plasma. The characteristic damping scales are: the horizon scale at neutrino decoupling, $M_\nu^{\rm FM} \approx 10^{-4} M_\odot$ in baryons, and the Silk mass at recombination, $M_\gamma^{\rm FM} \approx 10^{13} M_\odot$ in baryons. In contrast to fast magnetosonic waves, slow magnetosonic and Alfvén waves reach an overdamped regime during which the damping is not very efficient; further significant damping occurs once the radiation is free-streaming on the scale of the perturbation. The maximum damping scales for slow magnetosonic and Alfvén modes in general depend on the magnetic field strength and the direction of propagation with respect to the background magnetic field. At neutrino decoupling the damping scale is $M_\nu^{\rm A,SM} \approx 10^{-13} M_\odot B_9^3 \cos^3\theta$, the same for both types of modes. At recombination, if $B_9 < 1.7 \times 10^{-2}$, this scale is $M_\gamma^{\rm A,SM} \approx 10^6 M_\odot B_9^3 \cos^3\theta$, and if $B_9 > 1.7 \times 10^{-2}$, the damping scale for slow magnetosonic modes is different: $M_\gamma^{\rm SM} \approx 1 M_\odot \cos^3\theta$. The background magnetic field strength scaled to the present epoch is expressed in terms of $B_9 = (B_0/3 \times 10^{-9}{\rm Gauss})$, the current observational limit on the large scale magnetic field.

Our findings have various implications for cosmological magnetic fields. The dissipation of magnetic field energy into heat during the epoch of neutrino decoupling ensures that most magnetic field configurations generated prior to neutrino decoupling satisfy big bang nucleosynthesis constraints. The observed element abundances require that the energy density in magnetic fields be less than one-third of the photon energy density during nucleosynthesis [18,19]. Even if processes prior to neutrino decoupling generate magnetic fields with initial energy density comparable to the photon energy density, neutrino damping causes the magnetic energy density to decrease substantially relative to that of radiation by the time of nucleosynthesis.

Further dissipation before recombination lessens considerably the magnetic field energy in primordial magnetic fields available for generating galactic magnetic fields or density perturbations. The damping of fast magnetosonic modes implies that a sizable fraction of the magnetic energy density is erased up to the Silk scale.

Finally, although Alfvén and slow magnetosonic modes also undergo significant damping, their damping scales depend on the strength and the direction of the background magnetic field and are generally smaller than the damping scale for fast magnetosonic modes. As long as mode coupling is not effective, which we expect to be true for non-oscillating modes before recombination, magnetic energy density can be stored in Alfvén and slow modes on scales well below the Silk mass. The survival of these modes may be of significance to the formation of structure on relatively small scales. In particular, these modes may be responsible for fragmentation of early structures as well as seeding early star formation. We will further discuss the consequences of the cosmological evolution of MHD modes in a subsequent paper.

## ACKNOWLEDGMENTS

We thank B. Berger, J. Geddes, A. Konigl, R. Kulsrud, and R. Rosner for help throughout this project. We are particularly grateful to B. Chandran for alerting us to the existence of overdamped magnetohydrodynamic modes. This work was performed, in part, under the auspices of the US Department of Energy by the Lawrence Livermore National Laboratory under contract number W-7405-ENG-48 and DoE Nuclear Theory grant SF-ENG-48. It was also supported by DOE at University of Chicago, DOE and NASA at Fermilab. We also acknowledge the hospitality of the Aspen Center for Physics where some of this work was performed.

---

[1] E. R. Harrison, MNRAS **147**, 279 (1970); E. R. Harrison, MNRAS **165**, 185 (1973); C. J. Hogan, Phys. Rev. Lett. **51**, 1488 (1983); M. S. Turner and L. M. Widrow, Phys. Rev. D **30**, 2743 (1988); J. Quashnock, A. Loeb, and D. N. Spergel, ApJ **344**, L49 (1989); T. Vaschaspati, Phys. Lett. B **265**, 258 (1991); R. H. Brandenberger, A.-C. Davis, A. M. Matheson,

and M. Trodden, Phys. Lett. B **293**, 287 (1992); W. D. Garretson, G. B. Field, and S. M. Carroll, Phys. Rev. D **46**, 5346 (1992); B. Ratra, ApJ **391**, L1 (1992); B. Ratra, Phys. Rev. D **45**, 1913 (1992); A. D. Dolgov, Phys. Rev. D 48, 2499 (1993); A. D. Dolgov and J. Silk, Phys. Rev. D **47**, 3144 (1993); B. Cheng and A. V. Olinto, Phys. Rev. D **50**, 2421 (1994); K. Enqvist, P. Olensen, Phys. Lett. B **329**, 195 (1994); A. P. Martin and A.-C. Davis, Phys. Lett. B **360**, 71 (1995); T. W. B. Kibble and A. Vilenkin, Phys. Rev. D **52**, 679 (1995); M. Gasperini, M. Giovannini, and G. Veneziano, Phys. Rev. Lett. **75**, 3796 (1995); D. Lemoine and M. Lemoine, Phys. Rev. D **52**, 1955 (1995); G. Baym, D. Bödecker, and L. McLerran, Phys. Rev. D **53**, 662 (1996).

[2] J. Silk, ApJ **151**, 459 (1968).
[3] C. W. Misner, ApJ **151**, 431 (1968).
[4] S. Weinberg, ApJ **168**, 175 (1971).
[5] B. Cheng and A. V. Olinto, Phys. Rev. D **50**, 2421 (1994).
[6] S. Weinberg, *Gravitation and Cosmology*, 53, (New York: John Wiley & Sons, 1972).
[7] C. W. Misner and D. H. Sharp, Phys. Lett. **15**, 279 (1965).
[8] L. D. Landau and E. M. Lifshitz, *Fluid Dynamics*, 2nd ed., 505 (Oxford: Pergamon, 1975).
[9] J. D. Jackson, *Classical Electrodynamics*, 2nd ed., (New York: John Wiley & Sons, 1962)
[10] K. Jedamzik and G. M. Fuller, ApJ **423**, 33 (1994).
[11] P. J. E. Peebles, ApJ **142**, 1317 (1965).
[12] P. J. E. Peebles and J. T. Yu, ApJ **162**, 815 (1970).
[13] P. J. E. Peebles, ApJ **248**, 885 (1981).
[14] B. J. T. Jones and R. F. G. Wyse, MNRAS **205**, 983 (1983).
[15] S. A. Bonometto and F. Lucchin, MNRAS **187**, 611 (1979).
[16] W. H. Press and E. T. Vishniac, ApJ **236**, 323 (1980).
[17] P. P. Kronberg, Rep. Prog. Phys. **57**, 325 (1994).
[18] P. Kernan, G. Starkman, and T. Vachaspati, Phys. Rev. D **54**, 7202 (1996).
[19] B. Cheng, A. V. Olinto, D. Schramm, and J. Truran, Phys. Rev. D **54**, 4714 (1996).

## APPENDIX A: RADIATION DIFFUSION

This appendix contains the diffusion regime dispersion relations and their solutions. The dispersion relation for magnetosonic waves, expanded to first order in $\kappa'$, $\eta'$, and $\xi'$ (which corresponds to a first order expansion in $l_\gamma/\lambda$), is:

$$\begin{aligned}
&\omega^5(6\kappa'(1+R)+3\kappa'\tilde{B}_0^2)\\
&+i\omega^4\big((1+R)^2+\tilde{B}_0^2(1+R)\big)\\
&+\omega^3\Big(7\eta'(1+R)\left(\frac{k}{a}\right)^2+3\xi'(1+R)\left(\frac{k}{a}\right)^2+\kappa'(R^2-2)\left(\frac{k}{a}\right)^2+3\eta'\tilde{B}_0^2\left(\frac{k}{a}\right)^2+\kappa'\tilde{B}_0^2(R-2)\left(\frac{k}{a}\right)^2\\
&\qquad+\eta'\tilde{B}_0^2\cos^2\theta\left(\frac{k}{a}\right)^2+3\xi'\tilde{B}_0^2\cos^2\theta\left(\frac{k}{a}\right)^2-2\kappa'\tilde{B}_0^2\cos^2\theta\left(\frac{k}{a}\right)^2+2\frac{\dot{a}}{a}R(1+R)+\frac{\dot{a}}{a}\tilde{B}_0^2R)\Big)\\
&+i\omega^2\Big(-\frac{1}{3}(1+R)\left(\frac{k}{a}\right)^2-\tilde{B}_0^2(1+R)\left(\frac{k}{a}\right)^2-\frac{1}{3}\tilde{B}_0^2\cos^2\theta\left(\frac{k}{a}\right)^2\Big)\\
&+\omega\Big(-\eta'\left(\frac{k}{a}\right)^4-3\eta'\tilde{B}_0^2\left(\frac{k}{a}\right)^4-\kappa'\tilde{B}_0^2(1+R)\left(\frac{k}{a}\right)^4-\eta'\tilde{B}_0^2\cos^2\theta\left(\frac{k}{a}\right)^4\\
&\qquad-3\xi'\tilde{B}_0^2\cos^2\theta\left(\frac{k}{a}\right)^4+2\kappa'\tilde{B}_0^2\cos^2\theta\left(\frac{k}{a}\right)^4-\frac{1}{3}\frac{\dot{a}}{a}R\left(\frac{k}{a}\right)^2-\frac{\dot{a}}{a}\tilde{B}_0^2R\left(\frac{k}{a}\right)^2\Big)\\
&+i\frac{\tilde{B}_0^2\cos^2\theta}{3}\left(\frac{k}{a}\right)^4+iR\kappa'\frac{\dot{a}}{a}\tilde{B}_0^2\left(\frac{k}{a}\right)^4+3i\kappa'\eta'\tilde{B}_0^2\left(\frac{k}{a}\right)^6=0.
\end{aligned}\tag{A1}$$

Since the scales of interest are smaller than the horizon scale, we only keep $\dot{a}/a$ terms which are first order in $l_\gamma/d_{\rm H}$ and $\lambda/d_{\rm H}$. In addition, note that there are two terms in the last row which seem to be second order in the expansion variables, although for some slow magnetosonic waves for which $B_0\cos\theta$ is so small that $\tilde{B}_0^2\cos^2\theta \ll B_0^2\eta'\kappa'$ or $\tilde{B}_0^2\cos^2\theta \ll B_0^2\kappa'\dot{a}/a$, these terms play a crucial role in determining the damping rates for overdamped solutions.

We recover the dispersion relation for sound waves from the one for magnetosonic waves, if $B_0=0$, or if the magnetosonic wave propagates along the field lines, $\mathbf{k}\|\mathbf{B}_0$:

$$3\omega^3\kappa' + i\omega^2(1+R) + \omega\left[4\left(\frac{k}{a}\right)^2\eta' + 3\left(\frac{k}{a}\right)^2\xi' - (1-R)\left(\frac{k}{a}\right)^2\kappa' + \frac{\dot{a}}{a}R\right] - \frac{i}{3}\left(\frac{k}{a}\right)^2 = 0 \tag{A2}$$

The dispersion relation for Alfvén waves is:

$$3\omega^3\kappa' + i\omega^2\left(1 + R + \tilde{B}_0^2\right) + \omega\left(\frac{\dot{a}}{a}R + 3\eta'\left(\frac{k}{a}\right)^2\right) - i\tilde{B}_0^2\cos^2\theta\left(\frac{k}{a}\right)^2 = 0 \ . \tag{A3}$$

The solutions to the dispersion relations are presented using the following convention: the oscillatory part of the frequency is denoted by $\omega_0 = \mathrm{Re}\,\omega$, and the damping rate by $\omega_1 = \mathrm{Im}\,\omega$. For Alfvén waves the solutions are:

$$\begin{aligned} \omega_0 &= \pm\frac{1}{(1+R+\tilde{B}_0^2)}\sqrt{\tilde{B}_0^2(1+R+\tilde{B}_0^2)\left(\frac{k}{a}\right)^2 - \frac{1}{4}\left(\frac{\dot{a}}{a}\right)^2 R^2} \ , \\ \omega_1 &= \frac{1}{2(1+R+\tilde{B}_0^2)}\left[3\eta'\left(\frac{k}{a}\right)^2 + 3\kappa'\tilde{B}_0^2\cos^2\theta\left(\frac{k}{a}\right)^2\frac{1}{(1+R+\tilde{B}_0^2)} + \frac{\dot{a}}{a}R\right] \ . \end{aligned} \tag{A4}$$

For magnetosonic waves, a general solution for a non-dissipative fluid is:

$$\begin{aligned} \omega_0 = \pm\frac{v_s}{\sqrt{2}}\left(\frac{k}{a}\right)\Bigg[&\frac{1+R+3\tilde{B}_0^2(1+R)+\tilde{B}_0^2\cos^2\theta}{(1+R+\tilde{B}_0^2)} \\ &\pm\left(\frac{\left(1+R+3\tilde{B}_0^2(1+R)+\tilde{B}_0^2\cos^2\theta\right)^2}{\left(1+R+\tilde{B}_0^2\right)^2} - 12\tilde{B}_0^2\cos^2\theta\frac{(1+R)}{(1+R+\tilde{B}_0^2)}\right)^{\frac{1}{2}}\Bigg]^{\frac{1}{2}} . \end{aligned} \tag{A5}$$

This solution contains two magnetosonic solutions: fast magnetosonic, whose frequency is obtained by taking the plus sign, and slow magnetosonic, using the minus sign. For weak magnetic fields Eq. A5 may be expanded to second order in $B_0$, and the solutions become:

$$\omega_0^{\mathrm{FM}} = \pm v_s\left(\frac{k}{a}\right)\left(1 + \frac{3R+2}{2(1+R)}\tilde{B}_0^2\sin^2\theta\right) + O(B_0^4) \ , \tag{A6}$$

and

$$\omega_0^{\mathrm{SM}} = \pm v_A\left(\frac{k}{a}\right)\left(1 - \frac{3R+2}{2(1+R)}\tilde{B}_0^2\sin^2\theta\right) + O(B_0^5) \ . \tag{A7}$$

The imaginary (dissipative) parts of the magnetosonic frequencies, again to first order in $\dot{a}/a$, $\kappa'$, and $\eta'$, and to second order in $B_0$ are:

$$\omega_1^{\mathrm{FM}} = \left(\frac{k}{a}\right)^2\left[\frac{2}{1+R}\eta' + \frac{3}{2(1+R)}\xi' + \frac{R^2}{2(1+R)^2}\kappa'\right] + \frac{1}{2}\frac{\dot{a}}{a}\left(\frac{R}{1+R}\right) \tag{A8}$$

and

$$\omega_1^{\mathrm{SM}} = \frac{3}{2(1+R)}\left(\frac{k}{a}\right)^2\eta' + \frac{1}{2}\frac{\dot{a}}{a}\frac{R}{1+R} + \left(\frac{k}{a}\right)^2\left[\frac{3}{2}\kappa'\tilde{B}_0^2\sin^2\theta + \frac{3}{2}\kappa'\tilde{B}_0^2\cos^2\theta\frac{R}{(1+R^2)^2}\right] \tag{A9}$$

For sound waves Eq. A8 reduces to:

$$\omega_0 = \frac{1}{\sqrt{3(1+R)}}\left(\frac{k}{a}\right) \ , \tag{A10}$$

and

$$\omega_1 = \left(\frac{k}{a}\right)^2\left(\frac{R^2}{2(1+R)^2}\kappa' + \frac{2}{1+R}\eta' + \frac{3}{2(1+R)}\xi'\right) + \frac{1}{2}\frac{\dot{a}}{a}\frac{R}{(1+R)} \ , \tag{A11}$$

which reproduces the solution in Ref. [4] if the expansion is neglected ($\dot{a}/a = 0$ and $a = 1$).

## APPENDIX B: NEUTRINO FREE-STREAMING

During neutrino free-streaming, the dispersion relations are:

$$\omega^2(1+\tilde{B}_0^2) - \frac{3}{4}i\alpha\omega - \tilde{B}_0^2\cos^2\theta\left(\frac{k}{a}\right)^2 = 0 \tag{B1}$$

for Alfvén waves, and

$$\begin{aligned}
&\omega^4(1+\tilde{B}_0^2) - i\omega^3\frac{3}{4}\left[(2\alpha+\gamma)+(\alpha+\gamma)\tilde{B}_0^2\right] \\
&-\omega^2\left[\frac{1}{3}\left(\frac{k}{a}\right)^2 + \tilde{B}_0^2\left(\frac{k}{a}\right)^2 + \frac{\tilde{B}_0^2\cos^2\theta}{3}\left(\frac{k}{a}\right)^2 + \frac{9}{16}(\alpha^2+2\alpha\gamma+\alpha\gamma\tilde{B}_0^2)\right] \\
&+i\omega\left[\frac{1}{4}\alpha\left(\frac{k}{a}\right)^2 + \frac{3}{4}(\alpha+\gamma)\tilde{B}_0^2\left(\frac{k}{a}\right)^2 + \left(\frac{3}{4}\right)^2\alpha^2\gamma\right] + \frac{\tilde{B}_0^2\cos^2\theta}{3}\left(\frac{k}{a}\right)^2 + \frac{9}{16}\alpha\gamma\tilde{B}_0^2\left(\frac{k}{a}\right)^2 = 0
\end{aligned} \tag{B2}$$

for magnetosonic waves.

The solution to the dispersion relation for oscillatory Alfvén waves is:

$$\omega_{\rm osc}^{\rm A} = \pm\frac{v_{\rm A}\cos\theta}{\sqrt{1+\tilde{B}_0^2}}\left(\frac{k}{a}\right) + \frac{3}{8}i\frac{\alpha}{(1+\tilde{B}_0^2)}. \tag{B3}$$

The oscillatory magnetosonic solutions are expanded to first order in the dissipation coefficients $\alpha$ and $\gamma$, corresponding to the first order expansion in $\lambda/l_\nu$. This yields for fast magnetosonic waves:

$$\omega_{\rm osc}^{\rm FM} = \pm v_s(1+\tilde{B}_0^2\sin^2\theta)\left(\frac{k}{a}\right) + \frac{3}{8}i(\alpha+\gamma)\ , \tag{B4}$$

and for slow magnetosonic waves:

$$\omega_{\rm osc}^{\rm SM} = \pm v_A\cos\theta(1-\tilde{B}_0^2\sin^2\theta)\left(\frac{k}{a}\right) + \frac{3}{8}i(\alpha+3\tilde{B}_0^2\gamma)\ . \tag{B5}$$

The decay rates for overdamped slow manetosonic and Alfvén waves are given in the text in Eq. 74 and Eq. 75.

## APPENDIX C: PHOTON FREE-STREAMING

During photon free-streaming, the dispersion relation for Alfvén waves is:

$$\omega^2 - i\omega\left(\alpha+\frac{\dot{a}}{a}\right) - \frac{\tilde{B}_0^2\cos^2\theta}{R}\left(\frac{k}{a}\right)^2 = 0\ , \tag{C1}$$

and the dispersion relation for magnetosonic waves is:

$$\begin{aligned}
&\omega^5 - i\omega^4\left(2\alpha+\gamma+3\frac{\dot{a}}{a}\right) - \omega^3\left[c_s^2\left(\frac{k}{a}\right)^2 + \frac{\tilde{B}_0^2}{R}\left(\frac{k}{a}\right)^2 + \alpha^2 + 2\alpha\gamma + 2\frac{\dot{a}}{a}(2\alpha+\gamma)\right] \\
&+i\omega^2\left[\alpha\left(c_s^2+\frac{\tilde{B}_0^2}{R}\right)\left(\frac{k}{a}\right)^2 + \gamma\left(\frac{3}{5}c_s^2+\frac{\tilde{B}_0^2}{R}\right)\left(\frac{k}{a}\right)^2 + \frac{\dot{a}}{a}\left(c_s^2+2\frac{\tilde{B}_0^2}{R}\right)\left(\frac{k}{a}\right)^2 + \alpha^2\left(\gamma+\frac{\dot{a}}{a}\right) + 2\alpha\gamma\frac{\dot{a}}{a}\right] \\
&+\omega\left(\frac{k}{a}\right)^2\left[\frac{c_s^2\tilde{B}_0^2\cos^2\theta}{R}\left(\frac{k}{a}\right)^2 + \alpha\gamma\left(\frac{3}{5}c_s^2+\frac{\tilde{B}_0^2}{R}\right) + \gamma\frac{\dot{a}}{a}\left(\frac{3}{5}c_s^2+\frac{\tilde{B}_0^2}{R}\right) + \alpha\frac{\dot{a}}{a}\frac{\tilde{B}_0^2}{R}\right] - \frac{3}{5}i\gamma c_s^2\frac{\tilde{B}_0^2\cos^2\theta}{R}\left(\frac{k}{a}\right)^4 = 0.
\end{aligned} \tag{C2}$$

The magnetosonic dispersion relation has been derived to first order in $\dot{a}/a$, but without any approximation in the dissipative coefficients $\alpha$ and $\gamma$.

The oscillatory solution to the dispersion relation for Alfvén waves is:

$$\omega_{\rm osc}^{\rm A} = \pm c_{\rm A}\cos\theta\left(\frac{k}{a}\right) + \frac{i}{2}\left(\alpha + \frac{\dot a}{a}\right) . \tag{C3}$$

For fast magnetosonic waves in the adiabatic regime ($\mathrm{Re}\,\omega \gg \gamma,\alpha$) the oscillatory solution is:

$$\begin{aligned}
\omega_{\rm osc}^{\rm FM} &= \pm c_s\left(1+\frac{\tilde B_0^2}{2c_s^2 R}\sin^2\theta\right)\left(\frac{k}{a}\right) + i\left(\frac{\alpha}{2}+\frac{\gamma}{5}+\frac{\dot a}{a}\right) \qquad \text{for } c_s \gg c_A \\
\omega_{\rm osc}^{\rm FM} &= \pm c_A\left(1+\frac{c_s^2 R}{2\tilde B_0^2}\sin^2\theta\right)\left(\frac{k}{a}\right) + i\left(\frac{\alpha}{2}+\frac{\gamma}{5}\frac{c_s^2 R sin^2\theta}{\tilde B_0^2}+\frac{1}{2}\frac{\dot a}{a}\right) \quad \text{for } c_s \ll c_A
\end{aligned} \tag{C4}$$

and in the isothermal regime ($\gamma \gg \mathrm{Re}\omega \gg \alpha$) it is:

$$\begin{aligned}
\omega_{\rm osc}^{\rm FM} &= \pm\sqrt{\frac{3}{5}}c_s\left(1+\frac{5}{6}\frac{\tilde B_0^2}{c_s^2 R}\sin^2\theta\right)\left(\frac{k}{a}\right) + i\left(\frac{\alpha}{2}+\frac{c_s^2}{5\gamma}\left(\frac{k}{a}\right)^2+\frac{1}{2}\frac{\dot a}{a}\right) \quad \text{for } c_s \gg c_A \\
\omega_{\rm osc}^{\rm FM} &= \pm c_A\left(1+\frac{3}{10}\frac{c_s^2 R}{\tilde B_0^2}\sin^2\theta\right)\left(\frac{k}{a}\right) + i\left(\frac{\alpha}{2}+\frac{c_s^2}{2\gamma}sin^2\theta\left(\frac{k}{a}\right)^2+\frac{\dot a}{a}\right) \quad \text{for } c_s \ll c_A.
\end{aligned} \tag{C5}$$

The condition for adiabaticity is dependent on the strength of the magnetic field when $c_A \gg c_s$.
In the limit $B_0 = 0$, the above solutions give the solutions for sound waves:

$$\omega = \pm c_s\left(\frac{k}{a}\right) + i\left(\frac{\alpha}{2}+\frac{\gamma}{5}+\frac{\dot a}{a}\right) \tag{C6}$$

in the adiabatic regime ($c_s k/a \gg \gamma,\alpha$) and

$$\omega = \pm\sqrt{\frac{3}{5}}c_s\left(\frac{k}{a}\right) + i\left(\frac{\alpha}{2}+\frac{c_s^2}{5\gamma}\left(\frac{k}{a}\right)^2+\frac{1}{2}\frac{\dot a}{a}\right) \tag{C7}$$

in the isothermal regime ($\gamma \gg c_s k/a \gg \alpha$).
The oscillation frequency and the damping rate for slow magnetosonic waves in the adiabatic regime are:

$$\begin{aligned}
\omega_{\rm osc}^{\rm SM} &= \pm c_A\cos\theta\left(1-\frac{\tilde B_0^2}{2Rc_s^2}\sin^2\theta\right)\left(\frac{k}{a}\right) + i\left(\frac{\alpha}{2}+\frac{\gamma}{5}\frac{\tilde B_0^2\sin^2\theta}{c_s^2 R}+\frac{1}{2}\frac{\dot a}{a}\right) \quad \text{for } c_s \gg c_A \\
\omega_{\rm osc}^{\rm SM} &= \pm c_s\cos\theta\left(1-\frac{c_s^2 R}{2\tilde B_0^2}\sin^2\theta\right)\left(\frac{k}{a}\right) + i\left(\frac{\alpha}{2}+\frac{\gamma}{5}+\frac{\dot a}{a}\right) \qquad \text{for } c_s \ll c_A,
\end{aligned} \tag{C8}$$

and in the isothermal regime:

$$\begin{aligned}
\omega_{\rm osc}^{\rm SM} &= \pm c_A\cos\theta\left(1-\frac{5}{6}\frac{\tilde B_0^2}{Rc_s^2}\sin^2\theta\right)\left(\frac{k}{a}\right) + i\left(\frac{\alpha}{2}+\frac{1}{2}\frac{\dot a}{a}\right) \qquad \text{for } c_s \gg c_A \\
\omega_{\rm osc}^{\rm SM} &= \pm\sqrt{\frac{3}{5}}c_s\cos\theta\left(1-\frac{3}{10}\frac{c_s^2 R}{\tilde B_0^2}\sin^2\theta\right)\left(\frac{k}{a}\right) + i\left(\frac{\alpha}{2}+\frac{1}{2}\frac{\dot a}{a}\right) \quad \text{for } c_s \ll c_A,
\end{aligned} \tag{C9}$$

Note that all the solutions are derived for a background magnetic field whose energy density is much smaller than the energy density in photons ($\tilde B_0 \ll 1$).
In contrast to relativistic MHD there do exist non-relativistic, fast magnetosonic waves in the overdamped limit. The decay rates for the amplitudes of these overdamped fast magnetosonic waves are:

$$\begin{aligned}
\omega_{od}^{\rm FM} &= i\frac{3c_s^2}{5\alpha}\left(\frac{k}{a}\right)^2 \quad \text{for } c_s \gg c_A \\
\omega_{od}^{\rm FM} &= i\frac{c_A^2}{\alpha}\left(\frac{k}{a}\right)^2 \quad \text{for } c_s \ll c_A.
\end{aligned} \tag{C10}$$

The decay rates of overdamped slow magnetosonic and Alfvén waves are given in the text in Eq. 88 - Eq. 90.

## APPENDIX D: DAMPING SCALES

In this appendix we give the evolution of the damping scale as a function of temperature for Alfvén and slow magnetosonic modes in the early universe. The temperature dependence of the damping scale of fast magnetosonic waves is given in Section 4.1. Before neutrino decoupling, the damping scale for Alfvén and slow magnetosonic modes evolves as follows:

$$\lambda^{\mathrm{A,SM}} \simeq \begin{cases} 2\times 10^{20}\mathrm{cm}\left(\frac{T}{\mathrm{MeV}}\right)^{-\frac{5}{2}}\left(\frac{g_r}{10.75}\right)^{-\frac{3}{4}}\left(\frac{g_\nu}{5.25}\right)^{\frac{1}{2}}\left(\frac{g_l+g_q}{8.75}\right)^{-\frac{1}{2}} & \text{for } T>T_1 \\ 3\times 10^{15}\mathrm{cm}\,(B_9\cos\theta)^{\frac{5}{3}}\left(\frac{g_r}{10.75}\right)^{-\frac{1}{3}}\left(\frac{g_\nu}{5.25}\right)^{-\frac{1}{3}}\left(\frac{g_l+g_q}{8.75}\right)^{\frac{1}{3}} & \text{for } T_1>T>T_2 \\ 10^{18}\mathrm{cm}\,B_9\cos\theta\left(\frac{T}{\mathrm{MeV}}\right)^{-\frac{5}{2}}\left(\frac{g_r}{10.75}\right)^{\frac{1}{4}}\left(\frac{g_\nu}{5.25}\right)^{-\frac{1}{2}}\left(\frac{g_l+g_q}{8.75}\right)^{-\frac{1}{2}} & \text{for } T_2>T>T_3 \\ 10^{17}\mathrm{cm}\,B_9\cos\theta\left(\frac{g_r}{10.75}\right)^{-1}\left(\frac{g_\nu}{5.25}\right)^{\frac{1}{3}}\left(\frac{g_l+g_q}{8.75}\right)^{\frac{1}{3}} & \text{for } T_3>T. \end{cases} \tag{D1}$$

The damping scale at $T>T_1$ is approximately the same as the damping scale for fast magnetosonic modes, and represents the diffusion length of the decoupling particles. It is illustrated for photon decoupling by the dashed line on the left-hand-side of Fig. 3. The largest wavelength mode still damped by one e-fold during oscillatory diffusion becomes overdamped at temperature $T_1$:

$$\left(\frac{T_1}{\mathrm{MeV}}\right) = 80\ (B_9\cos\theta)^{-\frac{2}{3}}\left(\frac{g_r}{10.75}\right)^{-\frac{1}{6}}\left(\frac{g_\nu}{5.25}\right)^{\frac{1}{3}}\left(\frac{g_l+g_q}{8.75}\right)^{-\frac{1}{3}}, \tag{D2}$$

i.e. the temperature at which the oscillatory damping scale (diffusion length) and the overdamping length on the graph intersect.

Since the damping is inefficient during the overdamped diffusion phase, the largest length scale damped in diffusion represents the maximum damping scale, until further damping during free-streaming. Temperature $T_2$ represents the point when the overdamped free-streaming damping scale (equivalent to the dashed line on the right-hand-side of Fig. 3) exceeds the maximum scale damped so far,

$$\left(\frac{T_2}{\mathrm{MeV}}\right) = 10\ (B_9\cos\theta)^{-\frac{4}{15}}\left(\frac{g_r}{10.75}\right)^{\frac{7}{30}}\left(\frac{g_\nu}{5.25}\right)^{-\frac{1}{15}}\left(\frac{g_l+g_q}{8.75}\right)^{-\frac{1}{3}}. \tag{D3}$$

If this happens before decoupling, the damping scale grows further, and is now determined by the free-streaming damping scale. Finally, the largest length scale damped in free-streaming is the one which still damps by one e-fold before becoming oscillatory again, determined by the intersection of the dashed and the solid line on the right-hand-side of Fig. 3. This happens at:

$$\left(\frac{T_3}{\mathrm{MeV}}\right) = 5\left(\frac{g_r}{10.75}\right)^{\frac{1}{2}}\left(\frac{g_\nu}{5.25}\right)^{-\frac{1}{3}}\left(\frac{g_l+g_q}{8.75}\right)^{-\frac{1}{3}}. \tag{D4}$$

The final damping scale is determined by this transition; as it is given in Eq. D1 for $T<T_3$, it includes the scales damped during the transition itself. Note that for large magnetic field strength, with energy density approaching equipartition with radiation energy density ($B_9\approx 10^3$), and $\cos\theta\approx 1$, the maximum damping length scale is determined by damping during the oscillatory diffusion phase rather than during the overdamped free-streaming phase. In this case the damping scale of Alfvén and slow magnetosonic modes becomes similar to the damping scale of fast magnetosonic modes.

Around photon decoupling, the damping scale for Alfvén modes, and the damping scale for slow magnetosonic modes when $c_s>c_A$, have the same form:

$$
\lambda^{\rm A,SM} \simeq \begin{cases}
10^{26}{\rm cm}\left(\frac{\Omega_b h^2}{0.0125}\right)^{-\frac{1}{2}}\left(\frac{T}{0.25{\rm eV}}\right)^{-\frac{3}{2}} & \text{for } T > T_1 \\
10^{21}{\rm cm}\,(B_9\cos\theta)^3\left(\frac{\Omega_b h^2}{0.0125}\right) & \text{for } T_2 < T < T_1 \\
4\times 10^{23}{\rm cm}\,B_9\cos\theta\left(\frac{T}{0.25{\rm eV}}\right)^{-\frac{3}{2}}\left(\frac{\Omega_b h^2}{0.0125}\right)^{-\frac{1}{2}} & \text{for } T_{\rm EQ} < T < T_2, \\
2\times 10^{23}{\rm cm}\,B_9\cos\theta\left(\frac{T}{0.25{\rm eV}}\right)^{-\frac{5}{4}}\left(\Omega_0 h^2\right)^{-\frac{1}{4}}\left(\frac{\Omega_b h^2}{0.0125}\right)^{-\frac{1}{2}} & \text{for } T < T_{\rm EQ}.
\end{cases} \tag{D5}
$$

On the other hand, if $c_A > c_s$, the damping scale for slow magnetosonic modes evolves like:

$$
\lambda^{\rm SM} \simeq \begin{cases}
10^{26}{\rm cm}\left(\frac{\Omega_b h^2}{0.0125}\right)^{-\frac{1}{2}}\left(\frac{T}{0.25{\rm eV}}\right)^{-\frac{3}{2}} & \text{for } T > T_1 \\
10^{21}{\rm cm}\,(B_9\cos\theta)^3\left(\frac{\Omega_b h^2}{0.0125}\right) & \text{for } T_2' < T < T_1 \\
4\times 10^{21}{\rm cm}\,\cos\theta\left(\frac{T}{0.25{\rm eV}}\right)^{-\frac{3}{2}} & \text{for } T_{\rm EQ} < T < T_2'. \\
3\times 10^{21}{\rm cm}\,\cos\theta\left(\frac{T}{0.25{\rm eV}}\right)^{-\frac{5}{4}}\left(\Omega_0 h^2\right)^{-\frac{1}{4}} & \text{for } T < T_{\rm EQ}.
\end{cases} \tag{D6}
$$

The transition temperatures are determined by matter-radiation equality at $T_{\rm EQ} = 5.5\,{\rm eV}(\Omega_0 h^2)$, and by the last scale damped by one e-fold in oscillatory diffusion, which becomes overdamped at $T_1$,

$$
\left(\frac{T_1}{0.25{\rm eV}}\right) = 2\times 10^3 (B_9\cos\theta)^{-2}\left(\frac{\Omega_b h^2}{0.0125}\right)^{-1}, \tag{D7}
$$

and presents the largest damping scale until damping in free-streaming damps even larger scales, at $T < T_2$ with

$$
\left(\frac{T_2}{0.25{\rm eV}}\right) = 50 (B_9\cos\theta)^{-\frac{4}{3}}\left(\frac{\Omega_b h^2}{0.0125}\right)^{-1}, \tag{D8}
$$

or $T < T_2'$ with

$$
\left(\frac{T_2'}{0.25{\rm eV}}\right) = 2 B_9^{-2} (\cos\theta)^{-\frac{4}{3}}\left(\frac{\Omega_b h^2}{0.0125}\right)^{-\frac{2}{3}}. \tag{D9}
$$

However, if $T_2 < T_{\rm EQ}$ the damping scale of $10^{21}$cm $(B_9\cos\theta)^3$ $(\Omega_b h^2/0.0125)$ is valid until $(T/0.25{\rm eV}) = 2B_9^{-12/5}$ $\cos\theta^{-8/5}$ $(\Omega_b h^2/0.0125)^{-4/5}$ $(\Omega_0 h^2/0.0125)^{-1/5}$, after which it changes to $3\times 10^{21}$cm $\cos\theta$ $(T/0.25{\rm eV})^{-5/4}$ $(\Omega_0 h^2)^{-1/4}$.

The above equations are derived for the case in which the universe is radiation dominated during damping in oscillatory diffusion ($T_1 > T_{\rm EQ}$). This is always true for the background magnetic fields with $B_9 \leq 1$. Although for larger background magnetic fields the damping processes are the same, the temperature dependence of the diffusion damping scale and its time of overdamping might be different, resulting in a different final damping scale. For example, for $B_9\cos\theta \approx 10^3$ (or $v_{\rm A}\cos\theta \approx 1$), the oscillatory diffusion damping scale dominates up to recombination, and its evolution in the matter dominated era determines the damping scale at recombination.

Slow magnetosonic modes which propagate almost perpendicular to the background magnetic field have different damping scales due to the additional term in Eq. 61. However, this scale is substantially different from those given in the text only for modes with $\cos\theta < 0.03 B_9^{8/3}$, which makes the influence of this additional damping term on the overall damping of slow magnetosonic modes negligible.